Università degli Studi di Urbino Carlo Bo

Department of Biomolecular Science (DISB)

Ph.D. programme in: Biomolecular and Health Sciences

Cycle: XXXV

Pivotal role of ERO1α in the arsenite-dependent regulation of Ca^{2+} homeostasis and mitochondrial superoxide formation

ACADEMIC DISCIPLINE: BIO/14

Coordinator: Prof. Marco Bruno Luigi Rocchi

Supervisor: Prof. Andrea Guidarelli

Co-Supervisor: Prof. Orazio Cantoni

Ph.D. student: Andrea Spina

ACADEMIC YEAR
2021/2022

Index

Abstract

Arsenic (As) is a chemical element belonging to the group of metalloids. Arsenic compounds, widely diffused in nature and largely used in agrotechnical and industrial processes, represent a serious concern for the ecosystem and human health. Indeed, human exposure to arsenic compounds increases the incidence of a plethora of diseases and various types of cancer. At the molecular level, trivalent arsenic (Na_2AsO_3, arsenite) causes numerous deleterious effects in target cells, through its binding to protein thiols or *via* the intermediate formation of reactive oxygen species (ROS), in the mitochondrial respiratory chain and via NADPH oxidase activation. Experimental work performed in our laboratory has focused on the mechanisms regulating mitochondrial ROS formation, an event requiring direct effects of the metalloid in the respiratory chain and, most importantly, a significant increase in the mitochondrial concentration of Ca^{2+}. Studies on the mechanism whereby arsenite affects Ca^{2+} homeostasis provided evidence for an initial stimulation of the inositol 1,4,5-triphosphate receptor (IP_3R), maximally induced at low concentrations, and the subsequent activation of the ryanodine receptor (RyR). Interestingly, the release of the cation from the RyR was critical to promote mitochondrial superoxide ($mitoO_2^{\bullet-}$) formation. It follows that arsenite induces $mitoO_2^{\bullet-}$ formation only cells concomitantly expressing the IP_3R and the RyR (as undifferentiated-U937 cells or terminally differentiated C2C12 cells). These observations emphasize the relevance of the RyR in events associated with mitochondria ROS formation, possibly due to the close apposition of the RyR with these organelles. Interestingly, we also obtained evidence for the existence of critical regulatory mechanisms for RyR activation, different from conventional Ca^{2+}-induced Ca^{2+} release mechanisms. We found that low dose arsenite dependent Ca^{2+} release from the IP_3R, was responsible for the triggering of an endoplasmic reticulum (ER) stress response, leading to increased expression of ERO1α, which in turn critically regulated RyR activity. Interestingly, pharmacological inhibition of the activity or expression of ERO1α, or its genetic deletion, was associated with the prevention of Ca^{2+} release from the RyR and the ensuing mitochondrial accumulation of the cation necessary for the formation of $mitoO_2^{\bullet-}$. Under the same conditions, the above treatments/manipulations prevented the early DNA strand scission or late mitochondrial dysfunction and mitochondrial permeability transition (MPT)-dependent apoptosis. We subsequently identified an additional mechanism leading to increased ERO1α expression, mediated by $mitoO_2^{\bullet-}$-derived H_2O_2, that however failed to impact on Ca^{2+} homeostasis. Based on these findings, it appears that only the mechanism driven by IP_3R-derived Ca^{2+} increases the expression of ERO1α in the close vicinity of the RyR, possibly in the mitochondria associated membranes (MAMs).

In conclusion, direct stimulation of the IP_3R is critical for the triggering of the effects of arsenite on Ca^{2+} homeostasis. This event was associated with the triggering of an ER stress response leading to increased ERO1α expression, possibly in the MAMs, which mediated RyR activation and the ensuing mitochondrial Ca^{2+} accumulation, critical for induces $mitoO_2^{\bullet-}$ formation. Pharmacological inhibition of ERO1α activity or expression was therefore associated with prevention of induces $mitoO_2^{\bullet-}$ formation as well as with prevention of the ensuing geno- and cyto-toxic effects. As a final note, we identified an additional mechanism of ERO1α expression, which however failed to affect Ca^{2+} homeostasis, possibly due its localization in domains of the ER distal from the RyR and the mitochondria.

1. Introduction

1.1. Arsenic, uses and risks.

Arsenic is a chemical element with an atomic number of 33 belonging to the group of metalloids, with chemical proprieties between metal and non-metal. In nature, arsenic compounds are widely distributed, mostly as grey-metallic rocks or in their crystal form. Arsenic is found in about 320 different minerals (Chen et al., 2013). The metalloid is widely employed as wood preservative, in the production of glass, paper, textile and color pigments, in agriculture in insecticides, herbicides, and preservatives for animal food and water. As a final note, arsenic is also employed in the pharmaceutical and semiconductor fields.

The main source of arsenic compounds is represented by the mining industries (Eisler, 2004). Arsenic compounds are however extremely toxic and represents a threat for ecosystems and living beings. Its wide use over the last century has been linked to the impoverishment of natural biodiversity and the onset of various human and plant/animal diseases. For these reasons, the Agency for Toxic Substances and Disease Registry (ATSDR) of the U.S.A. has classified arsenic in the first position of the List of Hazardous Substances (ATSDR, 2022). In nature, arsenic compounds are divided into primary arsenic-bearing minerals and secondary arsenic-minerals (Drahota and Filippi, 2009). When primary minerals are exposed to atmospheric factors and surface or groundwaters, several reactions lead to the formation of secondary arsenic-minerals. The form of arsenic-anion (arsenide) or dianion (di-arsenide), or arsenic-sulfar-seni-deanion(s) belongs to the first category. The secondary arsenic-bearing minerals are rare in nature and the most important arsenic oxidation states of this category are +5 (arsenate), +3 (arsenite), –3 (arsine), and 0 (elemental) arsenic (Kaur et al., 2011). In the soil, arsenic is generally present as arsenite and arsenate and in the air is normally found as a mixture of arsenite and arsenate (Lim et al., 2014). A plethora of arsenic compounds is instead found in the water, due to its indiscriminate discharge in rivers from industries and agriculture. According to the Center for Disease Control and Prevention, USA, another underestimated source of the metalloid is represented by combustion process, natural or industrial (including smoke of cigarettes, engine smoke, or coal smoke for energy production). In smoke, arsenic is usually attached to very small particles.

1.2. Diseases related to arsenic contamination and clinical applications.

Arsenic contamination of the ground, air and water are well documented in various parts of the planet. According to a recently published article (Shaji et al., 2021), more than 230 million people worldwide are at risk of arsenic poisoning, in both developed or developing countries. The WHO estimates that in 2021, 140 million people in different 50 countries have been drinking water at levels higher than allowed.

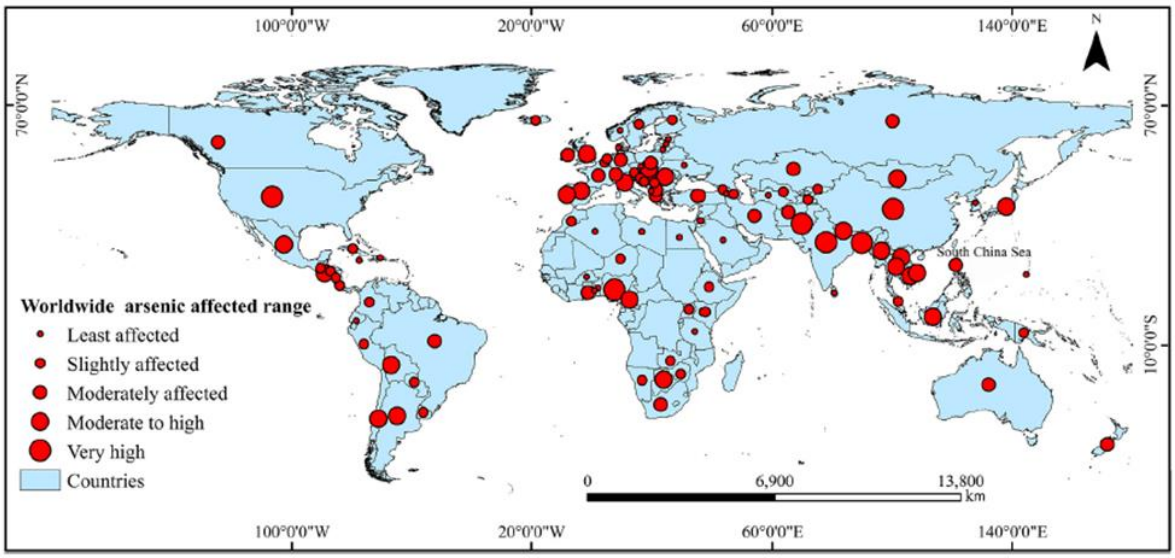

Figure 1: Arsenic risk map worldwide; (Shaji et al., 2021).

Arsenic is taken up by humans by inhalation, skin contact and, most importantly, by ingestion. In the bloodstream, arsenic binds to hemoglobin inside erythrocytes and is then distributed in different tissues. The symptoms of acute poisoning normally appear 30 min after ingestion, depending on the dose, and include metallic taste, garlic smell and difficulty in swallowing (Saha et al., 1999). Other symptoms are similar to those observed in other metal intoxications as palpitation, weakness with reddening skin, muscular pain, vomiting, severe nausea, colicky abdominal pain, and profuse diarrhea (Saha et al., 1999) (Ratnaike, 2003). Following the gastrointestinal phase, multisystem organ damage may occur, leading to death, or irreversible hepatic or renal failure (Tournel et al., 2011). Other symptoms related to the failure of the cardiocirculatory system are drowsiness and confusion often seen along with the development of a psychosis associated with paranoids, hallucinations, and delirium (Saha et al., 1999) (Ratnaike, 2003) (Tournel et al., 2011).

Low but chronic exposure to contaminated water, food, or air is linked to long-term effects. The major source of risk for human health is drinking and using contaminated water, including the use for animals and agriculture. The preclinical phase is often asymptomatic: high concentrations of arsenic in the bloodstream are mostly eliminated in the urine, but a little part is taken up in the skin, nails, or

hair (Saha et al., 1999) (Ratnaike, 2003) (Lim et al., 2014). It is estimated that the passage from the preclinical to clinical phase occurs within 6 months to 10 years or more, depending on the daily dose of exposure. The clinical manifestations are very heterogeneous and can be confounded with other diseases or viral infections; prevalent symptoms are anemia and leukopenia (decrease in leukocytes), but the most evident and recurring ones are at the skin level as melano-keratosis, dark pigmentation-diffuse and/or, dry, rough-spotted nodules in the palms and/or the soles (Saha et al., 1999) (Shaji et al., 2021), and leucomelanosis (depigmented spots in legs or trunk). Internal complications appear when organs are compromised, generally, the liver, bladder, spleen, and intestine, which can even evolve into many other collateral pathologies or organ failures (Chen et al., 1992) (Saha et al., 1999) (Flora, 2011). Arsenic exposure may also cause hypertension, peripheral arterial disease (Blackfoot disease), atherosclerosis, impaired microcirculation, coronary heart disease, and stroke (Flora, 2011). Lastly, the risk of developing a variety of neoplasms is remarkably increased (Basu et al., 2001) (Flora, 2011). The International Agency for Research on Cancer (IARC) defines arsenic as "carcinogenic to humans (Group 1): "There is enough evidence to conclude that it can cause cancer in humans" in 3 different volumes, 1980, 1987 and 2004 (IARC, 2012).

The toxic properties of the metalloid may have also therapeutical implications, as demonstrated by its use for centuries in the traditional Chinese medicine. *Salvarsan* was initially introduced in 1910 to cure syphilis and it is still used to treat trypanosomiasis (Council., 1999) (Waxman and Anderson, 2001). In 1931, the Boston hospital adopted arsenic trioxide (ATO) (since 1789 known as Fowler's solution) to treat myelogenous leukemia. Potassium arsenite was introduced in 1960 to treat many tumors in animals. With the recognition as cancerogenic in 1980, the use of arsenic-based therapy in clinics was significantly reduced (Council., 1999) (Waxman and Anderson, 2001). Nowadays, arsenical compounds are taking a new perspective based on novel discoveries in biology and medicine. In 2003 the U.S. Food and Drug Administration (FDA) approved the use of pure ATO in hematological malignancies, but its mechanism of action is still under study (Paul et al., 2022). Another inorganic arsenic-compound in use to treat melanoma and glioma is *Realgar* (red arsenic). Tryparsamide and other arsenic-compounds are also employed against *Trypanosoma brucei*, endemic in Africa (Paul et al., 2022). Sodium arsenite has been proposed for the treatment of lymphoma and other types of cancer Epstein–Barr virus derived. Numerous organic-arsenical compounds are still in the preclinical phase, showing fewer side effects for cancer treatments than inorganic ones. Furthermore, novel methylated-tri or pentavalent organic forms are currently under investigation as antibiotics and antiviral drugs (Paul et al., 2022). Thus, despite the high risk for human health, arsenic continue to maintain attraction for the development of novel therapeutical agents with diverse clinical applications.

1.3. Molecular mechanisms of arsenite toxicity.

Arsenic interacts with numerous biomolecules thereby inducing a wide spectrum of toxic effects and biochemical changes in different physiological functions. The effects of the metalloid can be directly mediated through its direct binding to specific target molecules, as proteins or the DNA. In alternative, the metalloid can mediate indirect effects *via* the intermediate formation of reactive oxygen species (ROS). It is important to note that basically all the arsenic forms are rapidly metabolized to arsenite (Minatel et al., 2018), an information emphasizing the relevance of the effects mediated by sodium arsenite or ATO.

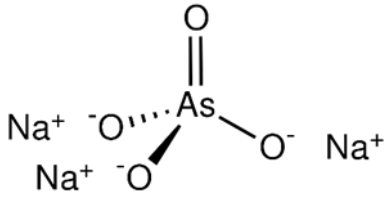

Figure 2: Structure of sodium arsenite.

Arsenite compounds are polar and their influx-efflux in cells from the plasma is mediated through membrane transporters such as AQP9, glucose transporter 2, and multidrug-resistant proteins (Flora, 2011). In the cytoplasm, depending on the cell type, arsenite is metabolized by reduction/methylation-oxidation reactions (biomethylation) as well as *via* conjugation with glutathione (GSH) (Habib G. M. et al., 2007). These processes lead to the formation of different metabolites which likely contribute to the overall toxic response (Minatel et al., 2018).

Direct effects:

The proteins directly affected by arsenite are more than 200 (Shen et al., 2013). Arsenite can replace the phosphate group (PO_4^{3-}) in proteins, an effect generally associated with their inactivation. Most importantly, the metalloid has a high affinity for sulfhydryl groups of proteins (H_2S) (Shen et al., 2013), an interaction often associated with loss of enzymatic activity (Sapra et al., 2015). Arsenic binding to protein also interferes with their normal folding (Sapra et al., 2015).

Arsenic binds to cysteine residues in many enzymes, some of which are also redox regulated. Arsenic hampers the antioxidant defense *via* inhibition of various enzymes, as the thioredoxins, an event contributing to the induction of oxidative stress (Shen et al., 2013).

Another critical aspect relates to the indirect genotoxic effects of arsenic compounds, which cannot be simply explained on the induction of ROS production (Batke et al., 2021). Indeed, arsenite can directly interact with the zinc finger, essential for the recognition of DNA, in the DNA repair

enzymes. This event synergizes with the formation of DNA lesions directly generated via the ROS-dependent mechanism (Roy et al., 2018).

Indirect effects:

The indirect effects of arsenite are mediated by the formation of ROS, which affect an array of signally pathway and promote a wide spectrum of toxic effects. The main ROS species produced by the metalloid are the superoxide anion ($O_2^{\bullet-}$), hydroxyl radical (-OH), hydrogen peroxide (H_2O_2), singlet oxygen ($^1O_2$), and peroxyl radicals (Valko et al., 2005) (Flora, 2011). The $O_2^{\bullet-}$ is considered a "primary" ROS, because it is characterized by a low reactivity and is eventually converted to "secondary" ROS (Valko et al., 2005). $O_2^{\bullet-}$ interacts with an extremely high affinity with nitric oxide (NO), thereby producing peroxynitrite, a very reactive species hampering many physiological functions. However $O_2^{\bullet-}$ is normally converted by the superoxide dismutases (SODs) to H_2O_2 (Liochev and Fridovich, 2007), thereby reducing the possibility of peroxynitrite formation. The SOD family is generally considered the main group of metalloproteases, that consists of 3 forms: SOD1, the cytoplasmic form with zinc and copper; SOD2, the mitochondrial form with iron or manganese; and SOD3 is extracellular (Wang et al., 2018). H_2O_2 is less reactive than $O_2^{\bullet-}$ but not harmless. Indeed, in the presence of divalent iron, H_2O_2 generates $OH^{\bullet-}$, highly reactive with nucleic acids (Winterbourn, 1995). Catalases detoxify H_2O_2 with concomitant formation of H_2O and O_2 (Goyal and Basak, 2010). GSH, thioredoxins and other antioxidants are also critically involved in the primary antioxidant defense to maintain an appropriate redox potential.

1.4. Arsenic effects in mitochondria

Irreversible changes in the redox state of the cell very rapidly lead to mitochondrial dysfunction. Mitochondria are a major site of ROS formation, in particular in complex I and III of the electron transport chain (ETC). Complex I releases $O_2^{\bullet-}$ in the mitochondrial matrix, whereas complex III, releases $O_2^{\bullet-}$ in the mitochondrial matrix as well as in intermembrane space. The activity of these complexes is affected by changes in redox homeostasis (Flora, 2011) (Magnani et al., 2020) (Fiorani et al., 2021). Arsenite interacts directly with mitochondrial proteins and promotes ROS formation. Arsenic interacts with succinic dehydrogenase (complex II of the mitochondrial respiratory chain) by inhibiting its activity (Hu et al., 2020). Arsenite also produces direct effects on Pyruvate Dehydrogenase (Hughes, 2002) (Jomova et al., 2011), thereby reducing the ATP levels. Arsenite promotes the onset of mitochondrial permeability transition (MPT), (Bonora and Pinton, 2014) that leads to further ROS production (Zorov et al., 2014) and cytochrome c release (Belzacq et al., 2001) (Habib G. M. et all., 2007) to drive the apoptotic process (Garrido et al., 2006).

1.5. Integrated stress response: Oxidative Stress trigger Endoplasmic Reticulum Stress.

Eukaryotic cells respond to intrinsic or extrinsic forms of stress by activating the integrated stress response (ISR) (Pakos-Zebrucka et al., 2016). The ISR is a combination of various pathways including a complex cytoprotective signaling which, at the start, reduces global protein synthesis and allows translation of a few selected mRNAs to promote cell recovery and survival (Pakos-Zebrucka et al., 2016) (Chong et al., 2017) (Almanza et al., 2019). When the correct homeostasis is compromised, a set of 'stress' signals is transmitted to the cytoplasm in other organelles, including the nucleus, to promote the expression of several targeted proteins (Pakos-Zebrucka et al., 2016) (Chong et al., 2017). Oxidative stress and reduction/oxidation imbalance in ER reduces the efficiency of protein folding and increases the production of misfolded proteins (Chong et al., 2017). ER plays a critical role in the synthesis, correct folding, and sorting of proteins, but it is also involved in many other functions, like the synthesis of phospholipids, cholesterol and steroids, the degradation of glycogen, detoxification processes and intracellular Ca^{2+} signaling (Almanza et al., 2019). Due to its function, the ER is particularly sensitive to ROS. The ER lumen has an oxidating potential, in contrast to the elevated reducing potential of the cytosol (Chong et al., 2017). Maintaining the correct redox homeostasis is critical for the oxidative folding, the acquisition of tertiary structure by polypeptide chain through the formation of covalent di-sulfidic crosslinks between specific cysteine residue side chains with oxidative reactions. O_2 and H_2O_2 are the main electron acceptors for the oxidative folding of proteins (Kosuri et al., 2012) (Braakman and Hebert, 2013). The oxidative folding is mediated by numerous proteins, as the chaperonin Heat-Shock proteins (Hsp) and PDI (Braakman and Hebert, 2013) (Chong et al., 2017). ERO1 is a primary enzymatic catalyst of biosynthetic disulfide bonds. ERO1α, the most conserved form and, ERO1β, described mostly in secretory cells (Sevier and Kaiser, 2008), are flavoproteins which sustain oxidative protein folding, by transferring electrons from cargo proteins *via* PDI to molecular oxygen, and yielding H_2O_2 as a by-product (Sevier and Kaiser, 2008) (Wang et al., 2014) (Shergalis et al., 2020). In turn, reduced PDI is re-oxidized by ERO1 α, *via* the FAD cofactor (Onda, 2013) (Shergalis et al., 2020). Studies with recombinant ERO1α demonstrate that for every disulfide bond generated, a peroxide molecule is formed and it is estimated that ERO1α activity in living cells may generate up to 25% of the cellular ROS produced during protein synthesis (Wang et al., 2014).

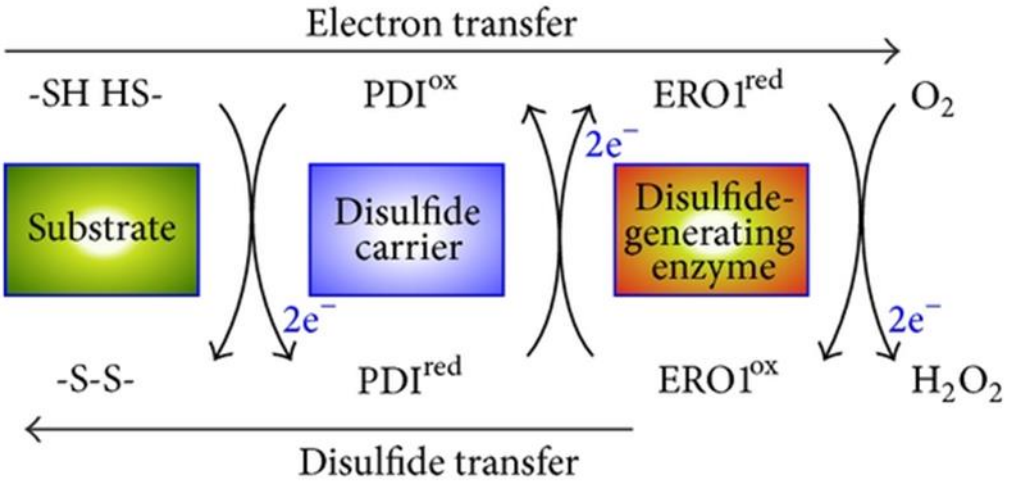

Figure 3: Physiological mechanism of action of ERO1; (Onda, 2013).

*These proteins are involved in oxidative folding and are extremely sensitive to the redox status of the ER. When the ER protein-folding capacity is exceeded, or if dysfunctional proteins cannot be properly folded, another ISR has triggered: the Unfolded Protein Response (UPR) improves the c folding capacity of the ER to restore homeostasis (Pakos-Zebrucka et al., 2016) (Chong et al., 2017) (Almanza et al., 2019).

1.6. Unfolded Protein Response: focus on ERO1α and altered Ca^{2+} homeostasis.

The UPR is a cellular stress response originating in the ER, mainly triggered by an excess of misfolded proteins. The UPR can be triggered by a severe ER stress or through the combination of low-level ER stress plus a "second hit" (Li et al., 2009). This signaling is generally cytoprotective, but, if the activation of UPR is prolonged, the cellular response switches from a pro-survival to pro-apoptotic signaling. Three major sensors ate normally implicated: inositol, requiring enzyme 1 (IRE1), protein kinase RNA-activated (PKR)-like ER kinase (PERK) and activating transcription factor 6 (ATF6) (Almanza et al., 2019). Their activation is mediated through the luminal domains of the sensors, BiP, which binds all three sensors in their inactive state (Almanza et al., 2019). When the level of unfolded protein load rises, BiP dissociates from these complexes exposing the active sites of the sensors, UPR sensors can directly feel the change in ER homeostasis, leading to their activation (Eletto et al., 2014a). All the UPR processes appear to be finely regulated, ER-resident PDI has a role, in particular, PDI5 and PDI6 that stop the action of the sensor by mediating a reduction of some disulfide bonds in specific cysteine residue (Eletto et al., 2014a) (Eletto et al., 2014b) (Almanza et al., 2019).

BiP

The ER-chaperone BiP binds to IRE1, PERK, and ATF6 in unstressed cells, and it dissociates from them during acute ER stress. It is considered the "fourth ER stress sensor" (Wang et al., 2014) and binds directly to the unfolded proteins. The ATPase-coupled domain stimulates conformational changes in its structure, allowing the binding and releasing of different substrates, but the precise mechanism behind such allosteric control remains to be investigated (Wang et al., 2014) (Almanza et al., 2019).

ATF6 signaling and IRE1 signaling

ATF6 is a member of a family of leucine zipper proteins. ATF6 exists in form of disulfide-bonded monomers, dimers, or oligomers exposed in the ER lumen (Almanza et al., 2019). BiP dissociation leads to its oxidization, and a monomeric reduced portion is released from the ER (Eletto et al., 2014a). The monomer moves to the Golgi where it is cleaved again and a fragment of ~ 400 amino acids are formed, named ATF6f. ATF6f is the active transcription factor that moves to the nucleus and induces the expression of UPR genes (Almanza et al., 2019) (Karagöz et al., 2019).

IRE1 is a single-pass transmembrane protein with a sensor in the ER lumen and a cytoplasmic effector. IRE1 coordinates the UPR through an unconventional splicing mechanism to encode the

transcription X-box binding protein 1 (XBP1) (Karagöz et al., 2019). BiP dissociation triggers IRE1 oligomerization and activation of its cytosolic kinase domain that induces a selective cleavage of dual stem loops within the XBP1 mRNA (Almanza et al., 2019). XBP1 directs the transcription of a wide range of targets including the expression of chaperones, foldases, and components of the ERAD pathway (Eletto et al., 2014b) (Almanza et al., 2019).

PERK Signaling

PERK has an ER luminal domain as well as a cytoplasmic kinase domain (Rozpedek et al., 2016). BiP detachment from PERK leads to its oligomerization, trans-autophosphorylation, and activation (Almanza et al., 2019). The main process of the active PERK is the phosphorylation of eIF2α (Wang et al., 2014). It is considered the main trigger of the UPR stress response, and it is the most conserved UPR sensor in all eucaryotic reign (McQuiston et al., 2017) (Almanza et al., 2019). Its position is critical for its activity. The portion of PERK in the ER lumen triggers the ER events, along with other ER stress sensors. The cytosolic domain can interact with other complexes to induce secondary pathways such as autophagy (Rozpedek et al., 2016) (McQuiston et al., 2017) (Almanza et al., 2019).

elF2α

The key factor for the induction of the ER stress response is the polypeptide chain initiation factor (eIF2), a heterotrimeric complex composed of an α-, β-, and γ-subunits. eIF2 binds GTP and initiator Met-tRNA to form eIF2-GTP-Met-tRNAi ternary complex (TC) (Clemens, 2001) (Rabouw et al., 2019). The TC, together with other translation initiation factors and the 40S ribosomal subunit, scans the mRNA for AUG start codons. Once found the correct base sequences, eIF2-bound GTP is hydrolyzed and eIF2-GDP is released from the translation complex (Rabouw et al., 2019b); to restart the cycle, GDP is replaced by eIF2β. In response to the stress, active PERK phosphorylates eIF2α, inhibiting eIF2β activity by stabilizing the association eIF2-GDP (Clemens, 2001) (Rabouw et al., 2019), thereby down-regulates protein synthesis (Almanza et al., 2019). On contrary, some transcripts are translated more efficiently after phosphorylation of elF2α, like the ubiquitously expressed activating transcription factor 4 (ATF4) and CHOP (a pro-apoptotic transcription factor) (Srivastava et al., 2018) (Almanza et al., 2019) (Rabouw et al., 2019).

ATF4

ATF4 is a transcription factor that targets genes, including itself, involved in amino acid transport, metabolism, protection from oxidative stress, autophagy and apoptosis, central in the UPR program

of gene expression (Srivastava et al., 2018). The phosphorylation mediated by PERK on eIF2α drives the translational of ATF4 from the cytoplasm to the nucleus (Shan et al., 2009).

CHOP

The transcription factor CHOP, also known as DNA damage-inducible gene 153 (GADD153) (Oyadomari et al., 2004), is targeted at the transcriptional level by ATF4. CHOP regulates a panel of genes involved in protein synthesis upon prolonged stress, including genes encoding amino acid transporters essential for intracellular GSH synthesis (Oyadomari et al., 2004) (Eletto et al., 2014a). One of the CHOP targets is ERO1α (Li et al., 2009) (Eletto et al., 2014b) (Karagöz et al., 2019).

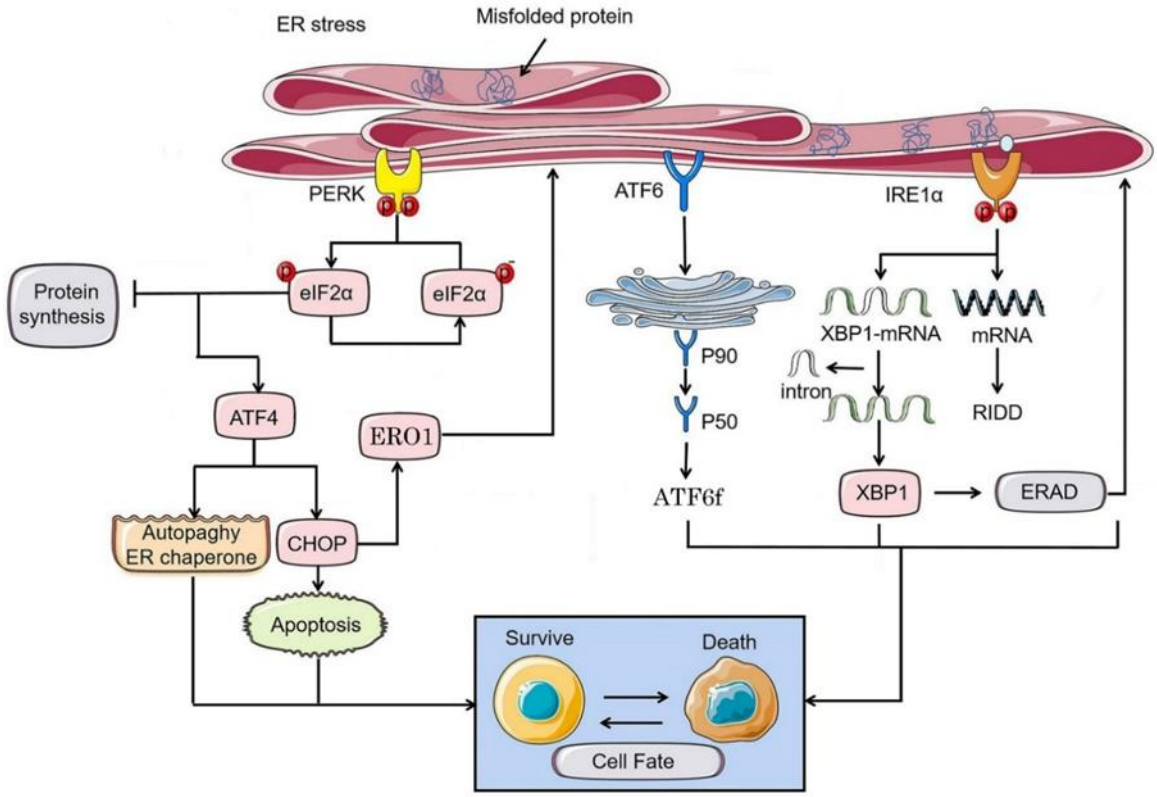

Figure 4: The UPR pathway

ERO1α

As previously discussed, ERO1α is a resident ER-oxidoreductase directly expressed by CHOP during the ER-stress response (Oyadomari et al., 2004) (Rozpedek et al., 2016) (Chong et al., 2017) (Almanza et al., 2019). In the last decade, numerous authors focused on the impact of this protein in the ISR, demonstrating that ERO1α is provided of multiple biological functions. (Li et al., 2009) have proposed the existence of a CHOP-ERO1α pro-apoptotic axis based on the activation of the Inositol

1,4,5-triphosphate receptor (IP_3R)1, releasing Ca^{2+} and causing mitochondrial dysfunction. This study was conducted in animal (mouse) models and in mouse fibroblasts (MEF) Wild Type (WT) as well as CHOP or ERO1α KO. Interestingly, lack of CHOP or ERO1α in cells treated with tunicamycin, an ER-stress inducer (Guha et al., 2017), or azetidine, another ER-stress inducer (Roest et al., 2018), prevented Ca^{2+} mobilization from the IP_3R and abolished the ensuing apoptosis. The mechanism(s) regulating IP_3R activation remain elusive. In another study (Chin et al., 2011) MEFs were grown in hypoxic conditions to express more ERO1α. It was found that the Ca^{2+} current was greater in WT- vs ERO1α KO cells. Also, with the use of Caffeine, a Ryanodine Receptor (RyR) (Meissner, 2017) agonist, the Ca^{2+} flux was significantly reduced in ERO1α KO cells than WT-cells. Thus, this study suggests a role for ERO1α in the regulation of Ca^{2+} release from both the IP_3R and RyR. Recently, ERO1α accumulation was observed in the MAMs, in the vicinity of the IP_3R (Anelli et al., 2012). Over-expression of ERO1α enhanced the rate of IP_3R oxidation leading to increased Ca^{2+} release from ER and to MPT (Anelli et al., 2012). Finally, a study suggested an effect of ERO1α on the RyR. The authors found that in rat myocytes, ERO1α interacts with the RyR thereby causing its hyperactivation under stress conditions (Hamilton et al., 2022).

1.7. Ca^{2+} induced mitochondrial ROS formation.

Ca^{2+} is a second messenger involved in the regulation of an array of signaling pathways, playing a central role in protein synthesis and trafficking, gene expression, cellular proliferation, metabolism, or apoptosis. The ER, as the main cellular compartment for Ca^{2+} storage, plays a pivotal role in the regulation of Ca^{2+} homeostasis. Consequently, the ER needs to maintain higher intraluminal Ca^{2+} concentrations and oxidizing redox potential than the cytoplasm (Almanza et al., 2019). The regulation of Ca^{2+} uptake and release processes is therefore essential for a correct ER function. Ca^{2+} uptake is mediated by the sarco- and endoplasmic-reticulum Ca^{2+}-ATPase (SERCA) family and the fraction of Ca^{2+} in the lumen is largely bound Ca^{2+} binding proteins (Kiviluoto et al., 2013) (Braakman et al., 2013) (Almanza et al., 2019). The main sites of Ca^{2+} storage in the ER are the IP_3R and the RyR. The cation is released from these sites *via* trans-membrane Ca^{2+} channels organized in 4 sub-units bounded together around a pore and presenting a portion in the ER lumen and the other one in the cytoplasm. The three isoforms of the IP_3R thus far been described (Bartok et al., 2019) are activated by 1,4,5 triphosphate. The RyR, is also found in three isoforms, distributed in the skeletal and cardiac muscles, as well as in other tissues. These channels release Ca^{2+} in response to the fraction of Ca^{2+} entering through the voltage dependent Ca^{2+} channels. The process is therefore defined as Ca^{2+}-induced Ca^{2+}-release (CICR) mechanism (Bootman et al., 2002). IP_3R or RyR channels are redox regulated, *via* poorly understood mechanisms involving oxidation of several cysteine residues. These channels, one of them or both, depending on the cell type, are expressed in the MAMs, in the vicinity of the mitochondria to optimize ER-mitochondria interactions and communication. This is of pivotal importance to allow mitochondrial Ca^{2+} uptake. Under these conditions, the cation is released to allow high concentration in microdomains sensed by the mitochondria, or more specifically, by the low affinity Mitochondrial Calcium Uniporter (MCU) (De Stefani et al., 2015).

An increase in the mitochondrial concentration of Ca^{2+} sustains ATP production, accompanied by the rise of NADH levels, NADPH, cofactors, and various modulators involved in oxidative metabolism and mitochondrial respiration (Duchen, 2000) (Giorgi et al., 2018) (Romero-Garcia, et al., 2019). In general, increased electron transport occurring under these conditions is paralleled by an increased formation of ROS. Ca^{2+} uptake is accompanied by increased mitochondrial membrane potential, but under specific conditions also promotes the triggering of mitochondrial permeability transition.

1.8. The effect of arsenite on Ca^{2+} homeostasis and mitochondrial ROS formation.

This topic has been actively investigated in our laboratory. The initial studies were performed in U937 cells, a versatile human pro-monocyte leukemia cell line. These cells, unlike other cell lines, express both the IP_3R and the RyR, are highly glycolytic, and express high affinity sodium-dependent vitamin C (ascorbic acid, AA) transporters (SVCT2) in both their plasma and mitochondrial membranes (Fiorani et al., 2015). Using specific exposure protocols (see below) AA concentrations can be significantly increased in the mitochondria to effectively scavenge $mitoO_2^{\bullet-}$ (Guidarelli et al., 2009). U937 cells can be differentiated to monocytes (D-U937), with a concomitant downregulation of the RyR (Guidarelli et al., 2009). U937 cells can also be easily made respiration-deficient (RD-U937), i.e., devoid of a functional ETC and hence unable to generate $mitoO_2^{\bullet-}$ (Guidarelli et al., 2009) (Guidarelli et al., 2016). RD-U937 cells, however, maintained intact mitochondria and mitochondrial potential, with the same capacity to accumulate Ca^{2+} as the mitochondria of their respiration proficient counterpart (RP-U937 cells). It was found that a low concentration (2.5 µM) of arsenite uniquely promotes $mitoO_2^{\bullet-}$ formation in RP-U937 cells. The dismutation product of $mitoO_2^{\bullet-}$, H_2O_2, mediates various downstream effects, including DNA strand scission, MPT, autophagy, and apoptosis (Guidarelli et al., 2016). Importantly, $mitoO_2^{\bullet-}$ also induces a cytoprotective signaling *via* nuclear factor erythroid 2 p45-related factor 2 (Nrf2), a transcriptional factor that promotes the expression of antioxidant enzymes and enhances GSH biosynthesis (Fiorani et al., 2018).

Further studies demonstrated that $mitoO_2^{\bullet-}$ formation requires direct effects of the metalloid in the ETC (Guidarelli et al., 2015) (Guidarelli et al., 2019) as well as the mitochondrial accumulation of Ca^{2+}. Using the same exposure protocol and the same cells, it was found that the metalloid increases the cytosolic Ca^{2+} concentrations ($[Ca^{2+}]_c$) *via* a ROS-independent mechanism suppressed by 2-aminoethoxydiphenyl borate (2-APB) (Berridge, 2016), an IP_3R antagonist, and partially reduced by Ryanodine (Ry), a RyR antagonist (Meissner, 2017). The fraction of Ca^{2+} released by IP_3R was however limited but nevertheless critical to stimulate the release of the cation from the RyR (Guidarelli et al., 2018). Interestingly, only the fraction of Ca^{2+} released by the RyR was taken up by the mitochondria, an observation emphasizing the existence of a close spatial relationship between the RyR and the mitochondria.

The above results have been validated in other cell lines (Guidarelli et al., 2021).

The mechanism of arsenite-dependent mito$O_2^{\bullet-}$ formation summarized in Fig 5 emphasizes the relevance of both direct and indirect effects of arsenite in the IP_3R and RyR, as well as the existence of a crosstalk between these channels mediated by yet unidentified mechanisms.

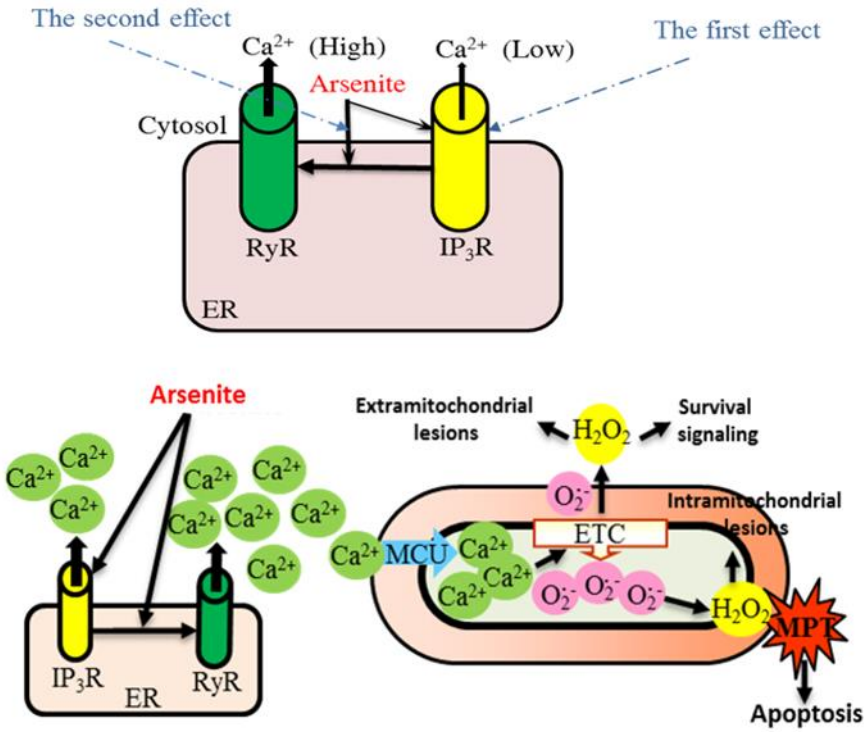

Figure 5: Mechanism whereby arsenite promotes Ca^{2+}-dependent mito$O_2^{\bullet-}$/H_2O_2 formation; (Guidarelli et al., 2019).

Aim of the thesis

We addressed the question of the specific contribution of the ER stress response, in particular of the enhanced ERO1α expression, in the regulation of Ca^{2+} homeostasis and ROS formation mediated by arsenite. More specifically, we investigated the specific regulation of the crosstalk between the IP_3R and RyR, which critically releases Ca^{2+} in microdomains sensed by the mitochondria to then promote mitochondrial ROS formation.

2. Materials and Methods

2.1. Chemicals.

Sodium arsenite ($NaAsO_2$), 2-aminoethoxydiphenyl borate (2-APB), ryanodine (Ry), ATP, caffeine (Cf), Ru360, L-ascorbic acid (AA), rotenone, hydrogen peroxide (H_2O_2), 3-(4,5-dimethylthiazol-2-yl)-2,5-diphenyltetrazolium bromide (MTT), Hoechst 33342, thapsigargin, as well most of the reagent and chemicals were purchased from Sigma-Aldrich (Milan, Italy). ISRIB and EN460 were obtained from Calbiochem (San Diego, CA). Cyclosporin A (CsA) was from Novartis (Bern, Switzerland). Fluo-4-acetoxymethyl ester, MitoSOX red and MitoTracker Red CMXRos, and Rhod 2-acetoxymethyl ester were purchased from Thermo Fisher Scientific (Milan, Italy).

Arsenite was prepared as 1 mM or 10 mM stock solution in saline A (8.182 g/l NaCl, 0.372 g/l KCl, 0.336 g/l $NaHCO_3$, and 0.9 g/l glucose, pH 7.4).

AA preparation and stability were detailed in ref. (Fiorani et al., 2015).

2.2. Antibodies.

The antibody against ERO1α was purchased from Novus Biologicals, LLC, USA (NB 100–2525). The antibody against β-actin was purchased from Bio-Rad, Hercules, CA, USA (AHP2417). The primary antibody against cytochrome c (7H8, sc-13560), myogenin (F5D, sc-122732), myosin (F59, sc32732), HSP-60 (H1, sc-13115), horseradish peroxidase-conjugated mouse secondary antibodies (sc-516102) or fluorescein isothiocyanate (FITC)-conjugated polyclonal goat anti-mouse (sc-2010) antibodies were purchased from Santa Cruz Biotechnology, Santa Cruz, CA, USA.

2.3. Cell culture.

U937 cells, pro-monocytic human myeloid leukaemia, define as respiration-proficient (RP)-U937 cells, were cultured in RPMI 1640 medium (Sigma-Aldrich) supplemented with 10% fetal bovine serum (FBS).

These RP-U937 cells were differentiated into monocytes (D-U937) by 4 days of growth in a culture medium supplemented with 1.3% dimethylsulfoxide, as indicated in (Guidarelli et al., 2009).

We also used respiration deficient (RD)-U937 cells. To obtain this cellular model, RP-U937 cells were cultured in RPMI medium containing 110 µg/ml pyruvate, 5 µg/ml uridine and 400 ng/ml

ethidium bromide for 4 days with medium changes every 2 days, as indicated in (Guidarelli et al., 2016).

C2C12, mouse myoblast, Wild Type (WT) and ERO1α Knock Out (KO) were cultured in high-glucose DMEM (6546-Sigma-Aldrich) supplemented with 10% heat-inactivated FBS and 2 mM L-glutamine. Differentiation to myotube was performed at 80-90% of confluence with supplementation of D-MEM with 1% heat-inactivated FBS for 4 days. Detail on the generation of ERO1α KO C2C12 was in (Varone et al., 2019).

All cells were cultured with penicillin (100 units/ml) and streptomycin (100 mg/ml) (Euroclone, Milano, Italy) at 37 °C in T-75 tissue culture flasks (Corning Inc., Corning, NY, USA) gassed with an atmosphere of 95% air-5% CO_2.

2.4 Real-time quantitative RT-PCR analysis.

Total RNA was isolated using the RNeasy Mini Kit (Qiagen, Hilden, DE) performing, following the manufacturer's instructions. One microgram of total RNA was reverse-transcribed and then, analyzed using the Applied Biosystems real-time PCR System and the ΔΔCt method as a statistics method. The mRNA levels were normalized with cyclophilin relative gene expression.

	Forward	Reverse
hs-ATF4	GGT TCT CCA GCG ACA AGG	TCT CCA ACA TCC AAT CTG TCC
hs-CHOP	CAT CAC CAC ACC TGA AAG CA	TCA GCT GCC ATC TCT GCA
hs-Cyclophilin	GAC CCA ACA CAA ATG GTTC C	TTT CACT TTG CC AAA CACC A

2.5. Sub-cellular fractionation and Western blot analysis.

Cells were lysed with RIPA buffer (Thermo Fisher Scientific) with the addition of 1 mM DTT, 1 mM Na_3VO_4, 1 mM NaF, 350 mM PMSF, 1% protease inhibitor complex, pH 7.5. In some experiments, the cells were processed to obtain the cytosolic and mitochondrial fractions, as described in (Yu et al., 2003). In other experiments, for non-reducing SDS-PAGE, cells were treated with 20 mM NEM to quench free thiols. The proteins were quantified with Bradford reagent (Bio-Rad) in SPECTRA Fluor Plus Microplate Reader Tecan (Tecan, Swiss). Then 30 µg of proteins were loaded in each lane, separated by polyacrylamide gel by vertical electrophoresis and transferred to polyvinylidene difluoride membranes. According to the experiments, the membranes were blocked and incubated

with primary antibodies against ERO1α, cytochrome c, β-actin, HSP-60, myosin, and myogenin. Immunoblots were processed with secondary antibodies anti-rabbit or anti-mouse depending on the primary antibodies used. The antibodies against β-actin and HSP-60 were employed to assess the equal loading of the lanes and to evaluate the purity of the fractions. Relative amounts of proteins were quantified by densitometric analysis using Image J software.

2.6. Measurement of cytosolic and mitochondrial Ca^{2+} levels.

Cells were grown in 35 mm tissue culture dishes containing an uncoated coverslip. In some experiments, cells were supplemented for 30 min before the end of the treatments with 4 μM Fluo-4 acetoxymethyl ester, a fluorescent probe used for measurement of the cytosolic Ca^{2+} or 10 μM Rhod-2 acetoxymethyl ester, a fluorescent probe employed for measurement the mitochondrial Ca^{2+}. In other experiments, the cells were supplemented for 20 min with Fluo-4 AM or Rhod-2 AM and exposed for an additional 10 min to ATP or Cf. Then, were washed three times and the fluorescence images were acquired with a BX-51 microscope (Olympus, Milan, Italy), equipped with a SPOT-RT camera unit (Diagnostic Instruments, Delta Sistemi, Rome, Italy) using an Olympus LCAch 40×/0.55 objective lens. The excitation and emission wavelengths were 488 and 515 nm for Fluo-4 and 540 and 590 nm for Rhod-2 with a 5-nm slit width for both emission and excitation. Images were digitally collected, with exposure times of 100–400 ms and processed for fluorescence determination at the single-cell level using the ImageJ software. Mean fluorescence values were determined by averaging the fluorescence values of at least 50 cells/treatment condition/experiment.

2.7. MitoSOX red fluorescence assay.

The cells were supplemented 30 min before the end of treatments with 5 μM MitoSOX Red, a fluorescent probe used for measurement of mito$O_2^{\bullet -}$. Then, were washed three times and fluorescence images were captured with a fluorescence microscope. The excitation and emission wavelengths were 510 and 580 nm for MitoSOX with a 5-nm slit width for both emission and excitation. Images were digitally collected, with exposure times of 100–400 ms and processed for fluorescence determination at the single-cell level using the ImageJ software. Mean fluorescence values were determined by averaging the fluorescence values of at least 50 cells/treatment condition/experiment.

2.8. Measurement of DNA single-strand breakage by the alkaline halo assay.

The formation of DNA single-strand breaks was determined using the alkaline halo assay. Details on the method, processing of fluorescence images and calculation of the experimental results were provided in (Cantoni and Guidarelli, 2008). Results are expressed as relative nuclear spreading factor

values and represent the ratio between the area of the halo (obtained by subtracting the area of the nucleus from the total area, nucleus + halo) and the nucleus, randomly selected cells/experiment/treatment condition at values of at least 50 cells.

2.9. Measurement of mitochondrial membrane potential.

Cells were grown in 35 mm tissue culture dishes containing an uncoated coverslip and exposed for 30 min with 50 nM MitoTracker Red CMXRos before the end of the treatment. The cells were washed three times and the fluorescence images were visualized using a fluorescence microscope. The excitation and emission wavelengths were 545 and 610 nm, with a 5 nm slit width for both emission and excitation. Images were digitally collected with, exposure times of 100–400 ms and processed for fluorescence determination at the single-cell level using the ImageJ software. Mean fluorescence values were determined by averaging the fluorescence values of at least 50 cells/treatment condition/experiment.

2.10. Immunofluorescence analysis.

After treatments, the cells were fixed for 1 min with 95% ethanol/ 5% acetic acid, washed with PBS, and blocked in PBS-containing bovine serum albumin (2% w/v) (30 min at room temperature). The cells were subsequently incubated with monoclonal anti-cytochrome c antibodies and stored overnight at 4 ◦C. Then were washed and incubated for 3 h in the dark with FITC-conjugated secondary antibody diluted 1:100 in PBS. The cells were examined with a fluorescence microscope.

2.11. Fluorogenic caspase 3 assays.

Caspase 3-like activity was determined fluorometrically by quantifying the release of amino-methylcoumarin (AMC) from cleaved caspase 3 substrate (Ac-DEVD-AMC). After protein quantification with Bradford reagent, 30 µg of protein were added to caspase 3 buffer: Hepes 100 mM, Sucrose 10% Chaps 0.1% EDTA 1 mM, pH 7.5 plus Ac - DEVD - AMC 0.4 mM. Fluorescence was determined at SPECTRA Fluor Plus Microplate Reader Tecan in excitation and 360 nM, emission 465 nM at 25 °C, for 3.40 h.

2.12. Cytotoxicity assay.

Cytotoxicity was performed with trypan blue exclusion assay. Briefly, an aliquot of the cell suspension was diluted 1:2 (v/v) with 0.4% trypan blue, and the viable cells (i.e., those excluding trypan blue) were counted with a hemocytometer. Toxicity was also determined using the MTT assay. In these experiments, the cells were supplemented with 25 µg/ml MTT in the last 30 min of the

treatments. Then, the cells were washed with PBS and the resulting formazan was extracted with 1 ml of dimethyl sulfoxide. Absorbance was read at 570 nm.

2.13. Analysis of apoptosis with the Hoechst 33342 assay.

Cells were incubated for 5 min with 10 µM Hoechst 33342 before the end of treatments and accurately washed three times with PBS. Fluorescence microscopy analysis was performed to determine the relative numbers of cells presenting evidence of chromatin condensation or fragmentation (apoptotic cells) and cells with homogeneously stained nuclei (viable cells).

2.14. Statistical analysis.

GraphPad Prism was used for statistical analysis. All quantitative data were presented as the mean ± standard deviation (SD). Statistically significant differences were obtained using an unpaired two-tailed student's t-test or by one-way analysis of variance (ANOVA) followed by Dunnett's test for multiple comparisons or two-way ANOVA followed by Bonferroni's test for multiple comparisons. The results represent the means ± SD calculated from at least three distinct experiments. *$P < 0.05$, **$P < 0.01$, as compared to untreated cells. #$P < 0.05$, ## $P < 0.01$, as compared to cells treated with arsenite.

3. Results

3.1. Arsenite induces ER stress and ERO1α expression.

The initial question addressed in my thesis work was whether arsenite triggers an ER-stress response under conditions associated with the exclusive formation of mito$O_2^{\bullet-}$. RP-U937 cells were therefore exposed for 6 h to 2.5 µM arsenite, a toxicity paradigm associated with mito$O_2^{\bullet-}$ formation (Guidarelli et al., 2019) (Guidarelli et al., 2021), and subsequently processed for ATF4 and CHOP mRNA expression analysis. We found that, under these conditions, the metalloid significantly increases ATF4 (Fig. 6A) and CHOP (Fig. 6B) mRNA levels, thereby providing clear evidence for the induction of an ER stress. This notion is also consistent with the observation that 2.5 µM arsenite causes an about threefold increase in ERO1α protein levels (Fig. 6C).

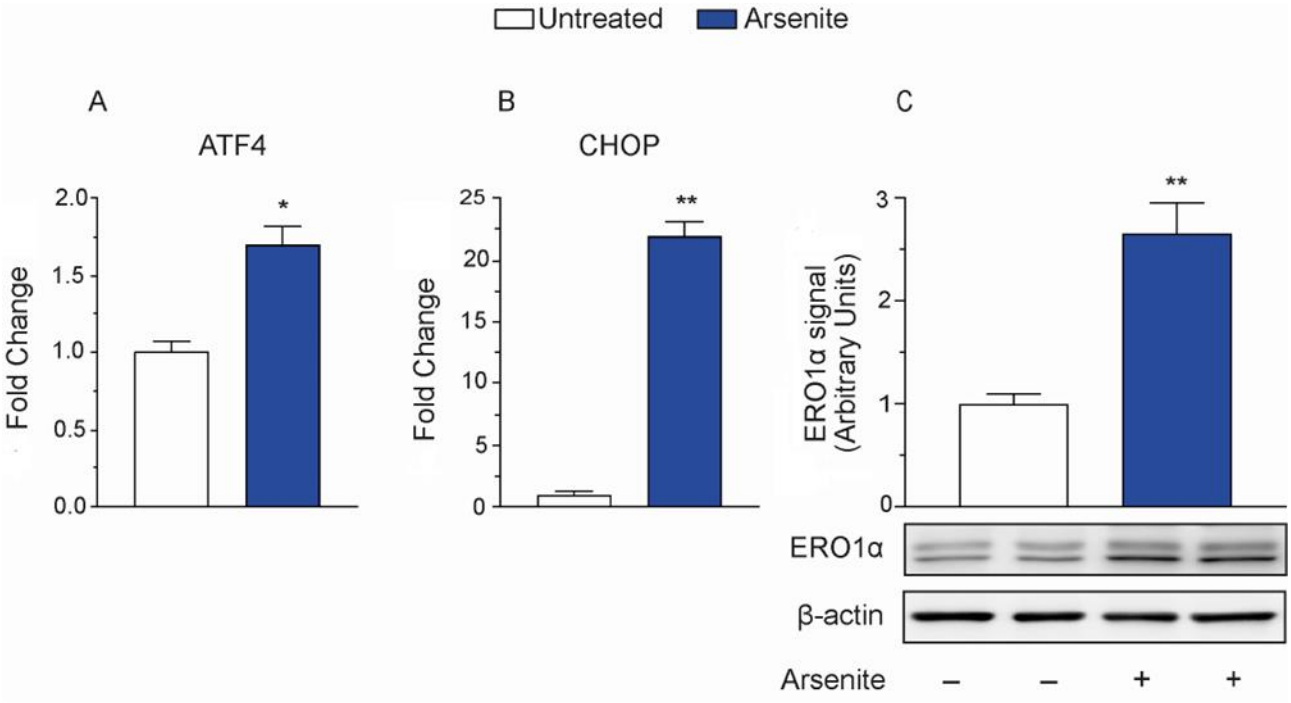

Figure 6: Arsenite induces ER stress and ERO1α expression.

RP-U937 cells exposed for 6 h to 2.5 µM arsenite were analyzed for ATF4 (A) and CHOP (B) mRNA expression, as well as for ERO1α (C) protein expression. Anti-β-actin antibody was used as a loading control. Results represent the means ± SD calculated from three separate experiments. *P < 0.05; **P < 0.01 compared with untreated cells (ANOVA followed by Dunnett's test).

In order to investigate the role of ERO1α in the cellular responses to the above toxicity paradigm, we decided to employ EN460, which interacts with the reduced form of ERO1α thereby preventing its reoxidation and inhibiting its activity (Blais et al., 2010).

It is important to note that in untreated RP-U937 most of ERO1α is in a reduced form, as indicated by SDS-PAGE analysis performed under reducing and non-reducing conditions (lines 1 and 2 in Fig. 7A). Exposure to EN460 (10-50 μM) caused the accumulation of disulfide bounded ERO1α, represented by the higher molecular weight band (compare line 3, 4, 5 in Fig. 7A), instead not observed under reducing conditions (Fig. 7B).

These results are in keeping with the notion that, even at lowest concentration tested (10 μM), EN460 inhibits ERO1α activity. Further analyses revealed that a 6 h exposure to 10 μM EN460 fails to promote loss of viability (Fig. 7C) or apoptotic chromatin fragmentation/condensation (Fig. 7D), instead detected in cells respectively exposed for 2 h to 50 μM (Fig. 7C) or for 6 h to 25 μM of H_2O_2 (Fig. 7D).

Next, we investigated the effects of EN460 on Ca^{2+} homeostasis. For this purpose, the cells were exposed for 6 h to EN460 with the further addition of ATP, an IP_3 releasing agonist (Berridge, 1993) or Cf, a RyR agonist (Meissner, 2017b) in the last 10 min, to then determine the Fluo-4 and Rhod-2 fluorescence responses, respectively indicative of the $[Ca^{2+}]_c$ and $[Ca^{2+}]_m$. As shown in Fig. 7, the increases in cytosolic (E) and mitochondrial (F) Ca^{2+} were identical in cells treated with ATP, or Cf, alone or in combination with EN460.

The results illustrated in this section indicate that a 6 h exposure of RP-U937 cells to 2.5 μM arsenite leads to an ER stress response associated with a significant expression of ERO1α. We also report the conditions to specifically inhibit ERO1α activity in the absence of toxic effects or other indirect or direct effects on Ca^{2+} homeostasis.

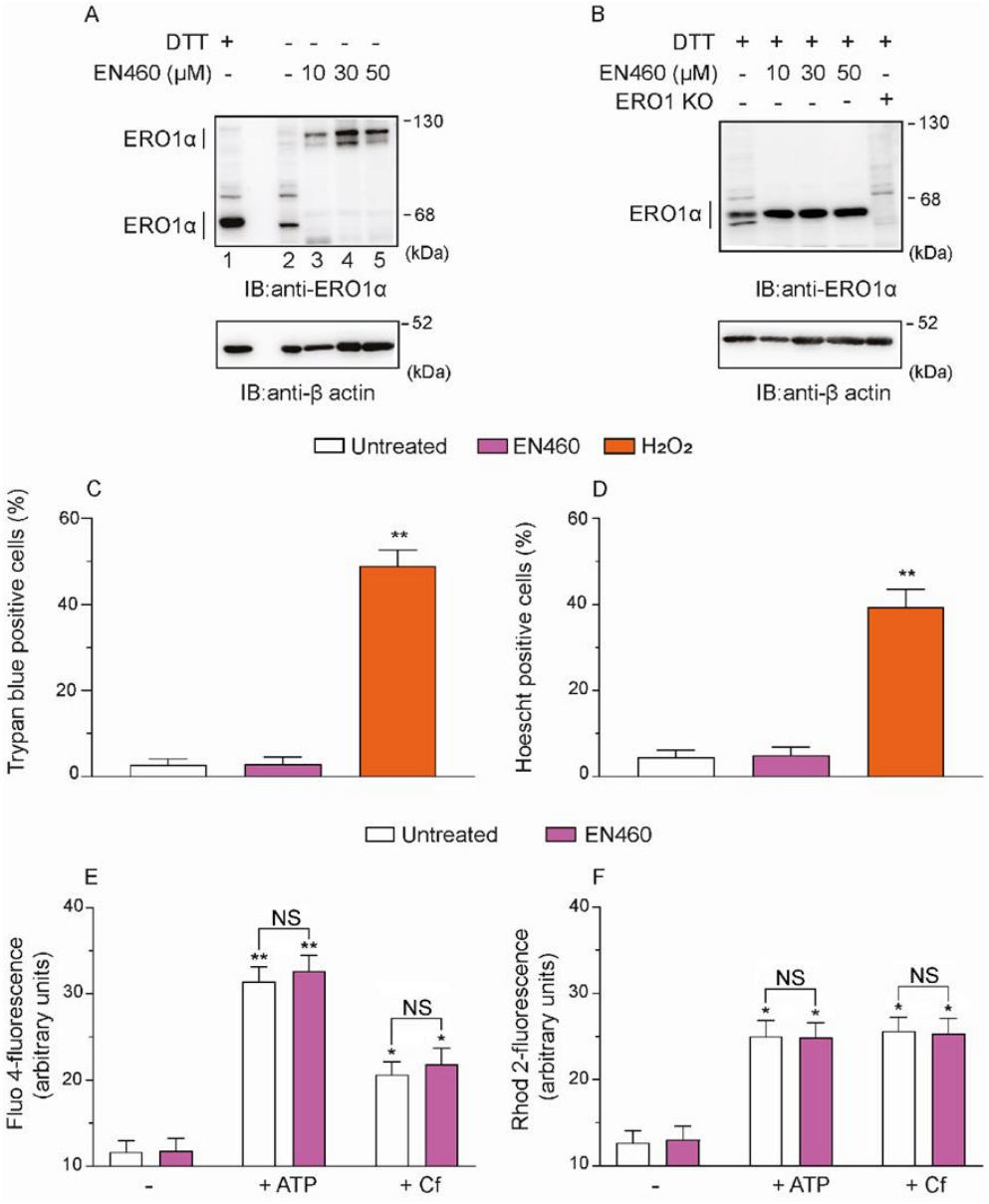

Figure 7: Activity and selectivity of EN460 as an ERO1α inhibitor.

RP-U937 cells were incubated for 6 h with 10, 30 or 50 µM EN460, washed and lysed in the presence of 20 mM NEM. Proteins were resolved on a non-reducing SDS-PAGE (A, the lanes between 1 and 2 is empty), or in a reducing SDS-PAGE after adding 100 mM DTT to the sample buffer (B). Anti-β-actin antibody was used as a loading control. In other experiments, cells exposed for 6 h to 10 µM EN460 were analyzed for cell viability with the trypan blue exclusion (C) and Hoechst (D) assays. Positive controls: 150 µM H_2O_2 for 2 h (C) or 25 µM H_2O_2 for 6 h (D). Finally, cells exposed for 6 h to 10 µM EN460 were washed, re-suspended in fresh culture medium, loaded (20 min) with Fluo 4 (E), or Rhod 2 (F), and subsequently incubated for 10 min with 100 µM ATP or 10 mM Cf. After treatments, the cells were analyzed for their respective fluorescence responses. Results represent the means ± SD calculated from three separate experiments. *P < 0.05; **P < 0.01 compared with untreated cells (ANOVA followed by Dunnett's test). (NS, no significant difference).

3.2. Pharmacological inhibition of ERO1α mimics the effects of ryanodine on Ca^{2+} mobilization and mitochondrial accumulation, as well as on ROS formation induced by arsenite.

Work performed in our laboratory (Guidarelli et al., 2021) has shown that a 6 h exposure of RP-U937 cells to 2.5 μM arsenite increases mito$O_2^{\bullet-}$ emission *via* a mechanism blunted by 2-APB, an IP_3R antagonist (Berridge, 2016), and partially inhibited by Ry, a RyR antagonist (Meissner, 2017) (Fig. 8A). In D-U937 devoid of RyR (Guidarelli et al., 2009), the metalloid caused a limited increase in the $[Ca^{2+}]_c$, comparable to that detected in RP-cells supplemented with Ry, *via* a mechanism sensitive to 2-APB (Fig. 8B). Interestingly, EN460, recapitulated the effects (Fig. 8A), or lack of effects (Fig. 8B), of Ry in both RP-U937 and D-U937 cells, respectively.

Next, we moved to experiments measuring mitochondrial Ca^{2+} accumulation mediated by arsenite in RP-U937, which, as previously shown (Guidarelli et al., 2019) (Cantoni et al., 2021), is sensitive to 2-APB or Ry (Fig. 8C), and not observed in D-U937 (Fig. 8D). EN460, suppressed the rise of $[Ca^{2+}]_m$ evoked by the metalloid in RP-U937 (Fig. 8C) and failed to promote effects in D-U937 (Fig. 8D).

In RP-U937, mitochondrial accumulation of Ca^{2+} was associated and critically connected with mito$O_2^{\bullet-}$ formation (Guidarelli et al., 2019) (Cantoni et al., 2021): this response was prevented by 2-APB, or Ry (Fig. 8E), and not observed in D-U937 (Fig. 9F). EN460, abolished mito$O_2^{\bullet-}$ formation detected in RP-U937 (Fig. 8E).

Collectively, the above results strongly suggest the involvement of ERO1α in the mechanisms associated with deregulation of Ca^{2+} homeostasis induced by arsenite. In addition, the results presented are consistent with the possibility that ERO1α plays a pivotal role in the phase of RyR activation after the initial stimulation of Ca^{2+} release from the IP_3R. As a final note, these findings are also important to understand the molecular bases of mito$O_2^{\bullet-}$ formation since this event is Ca^{2+} dependent and mitochondrial Ca^{2+} accumulation ensues because of Ca^{2+} mobilization from the RyR.

3.3. Pharmacological inhibition of Ca^{2+} mobilization blunts ERO1α expression induced by arsenite.

We investigated the mechanism whereby arsenite induces ERO1α expression and more specifically tested the role of Ca^{2+}. It was interesting to observe that in RP-U937 cells ERO1α expression was prevented by 2-APB and partially inhibited by Ry (Fig. 8G). Interestingly, EN460 recapitulated the effect of Ry. However, the low increase in ERO1α expression mediated by arsenite in D-U937 cells, while abolished by 2-APB, was insensitive to Ry or EN460 (Fig. 8H).

We therefore conclude that ERO1α expression induced by arsenite is critically regulated by Ca^{2+} release from the IP_3R and further amplified by the fraction of the cation released by the RyR, which, as demonstrated above, is activated *via* an ERO1α dependent mechanism. Thus, the Ry-sensitive fraction of ERO1α expression was also ERO1α -dependent.

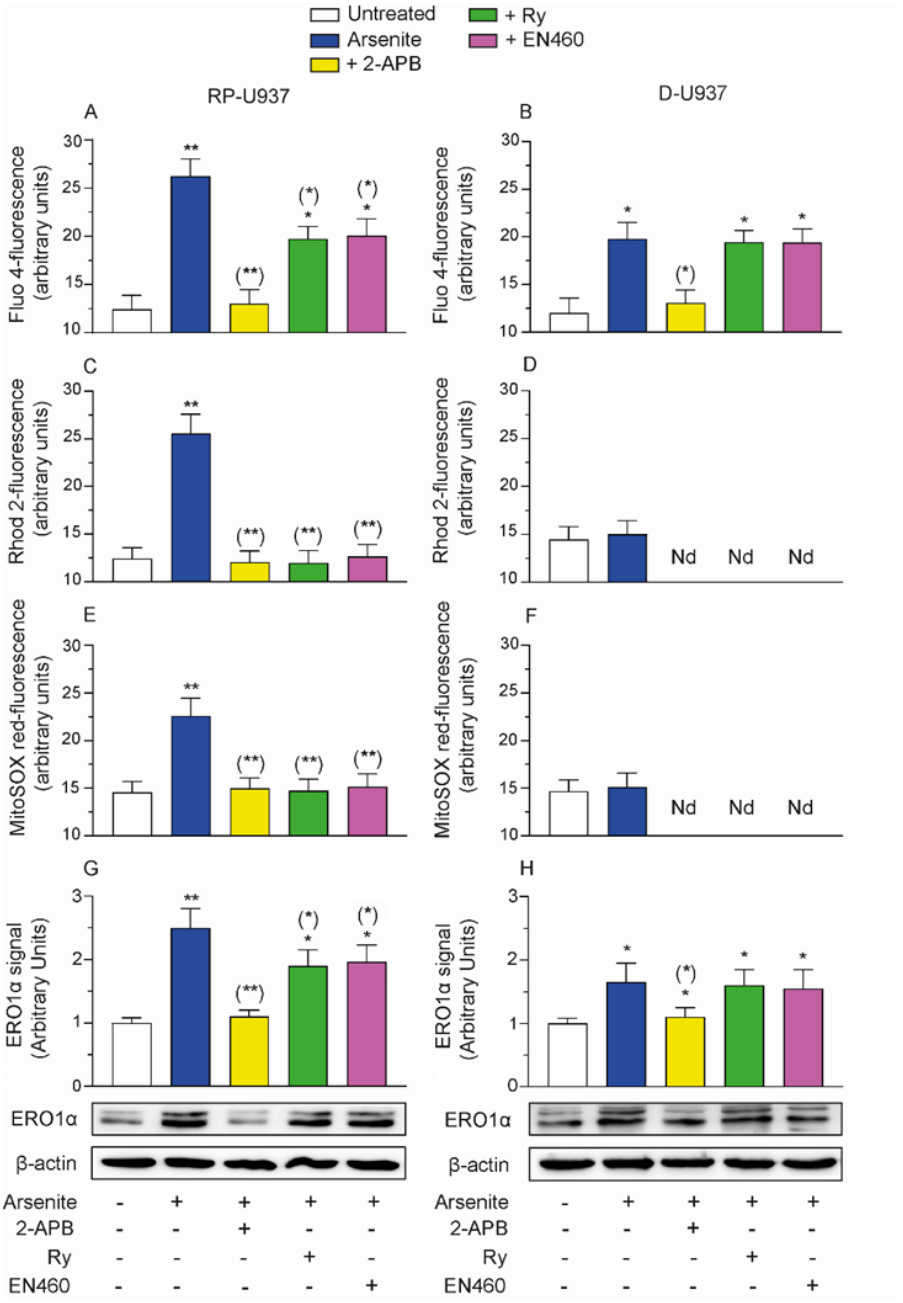

Figure 8. EN460 recapitulates the effects of ryanodine on $[Ca^{2+}]c$, $[Ca^{2+}]m$ and mitochondrial superoxide formation.

RP-U937 (A, C, E, G) and D-U937 (B, D, F, H) cells were pretreated for 5 min with the vehicle, 50 µM 2-APB, 20 µM Ry or 10 µM EN460 and incubated for 6 h with the further addition to arsenite. After treatments, the cells were analyzed for Fluo 4- (A, B), Rhod 2- (C, D), MitoSOX red- (E, F) fluorescence, as well as ERO1α (G, H) protein expression. Anti-β-actin antibody was used to provide an internal loading control. The results represent the means ± SD calculated from at least three distinct experiments. (N.d., not detectable). *P < 0.05, **P < 0.01, as compared to untreated cells. (*) P < 0.05, (**) P < 0.01, as compared to cells treated with arsenite (ANOVA followed by Dunnett's test).

3.4. Validation of the proposed mechanism(s) using WT C2C12 and ERO1α KO myotubes.

To validate our previous findings, entirely based on the use of RP- and D-U937 cells and of a single inhibitor of ERO1α activity, EN460, we decided to perform experiments in a different cellular system which, while characterized by a similar functional organization of the IP_3R/RyR/mitochondria network, present remarkably different characteristics. We used terminally differentiated murine myotubes (WT D-C2C12), which, as previously reported (Guidarelli et al., 2021) respond to ATP or Cf with mechanisms of Ca^{2+} release comparable to those observed in RP-U937 cells. Most importantly, these cells also responded to arsenite with increases in the $[Ca^{2+}]_c$ and $[Ca^{2+}]_m$, as well as with $mitoO_2^{\bullet-}$ formation, like those detected in RP-U937 cells.

Next, we performed experiments using ERO1α KO D-C2C12, previously generated with the CRISPR-Cas9 technology by (Varone et al., 2019). Firstly, we demonstrated that the extent of differentiation of WT and ERO1α KO D-C2C12 was remarkably similar in terms of morphology (Fig. 9A), and myogenin or myosin expression (Fig. 9B). Secondly, we showed that arsenite increases ERO1α expression in WT D-C2C12, *via* a mechanism suppressed by 2-APB and largely reduced by Ry, or EN460, with no evidence of ERO1α expression in both the untreated and arsenite-treated KO counterpart (Fig. 9C).

Arsenite increased the $[Ca^{2+}]_c$ (Fig. 9D), $[Ca^{2+}]_m$ (Fig. 9E) and $mitoO_2^{\bullet-}$ formation (Fig. 9F) in WT D-C2C12 and these effects were prevented by 2-APB. Ry and EN460 partially inhibited the increase of the $[Ca^{2+}]_c$ (Fig. 9D) and suppressed the mitochondrial accumulation of the cation and the ensuing $mitoO_2^{\bullet-}$ formation (Fig. 9E, F). ERO1α KO D-C2C12 instead responded to arsenite with a limited rise of the $[Ca^{2+}]_c$ (Fig. 9D), sensitive to 2-APB and insensitive to Ry, or EN460. Furthermore, the metalloid failed to increase the $[Ca^{2+}]_m$ (Fig. 9E) or to promote $mitoO_2^{\bullet-}$ formation (Fig. 9F) in these cells.

Collectively, the results presented in this section corroborate the above findings obtained in RP-U937 cells by showing that identical mechanisms mediate ERO1α expression in a completely different cell line. Our previous conclusion was based on inhibitor studies, in particular using EN460, is validated with the use of ERO1α KO cells, in which there was no evidence of ERO1α expression in both naïve end arsenite-treated cells.

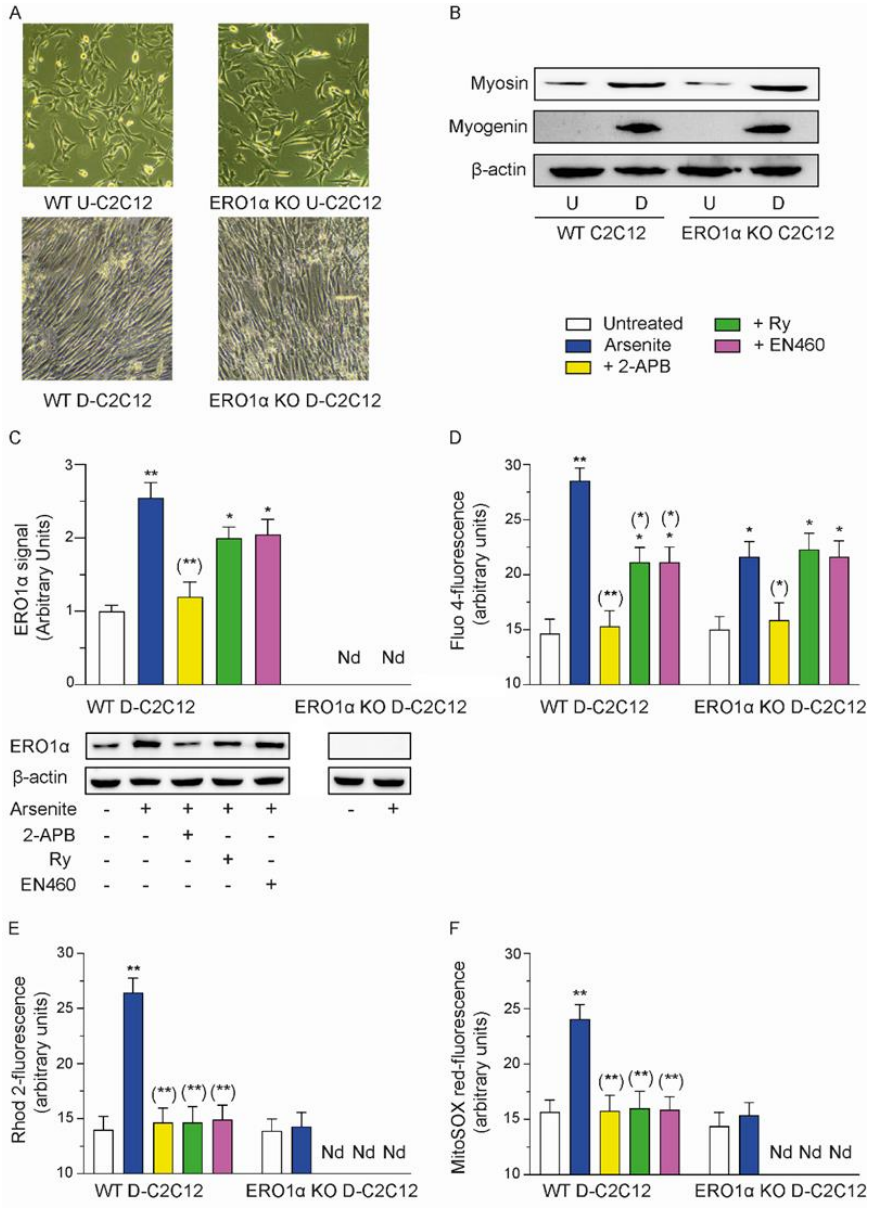

Figure 9. Validation of the proposed mechanisms in WT and ERO1α KO C2C12 myotubes.

(A) Representative images of C2C12 myoblasts (WT U-C2C12 and ERO1α KO U-C2C12) and day 4 C2C12 myotubes (WT D-C2C12 and ERO1α KO D-C2C12). (B) Western blot analysis for myogenin and myosin expression in myoblasts and myotubes. Anti-β-actin was used as a loading control. WT and ERO1α KO D-C2C12 cells were pretreated for 5 min with the vehicle, 2-APB, Ry or EN460 and incubated for a further 6 h in the presence of arsenite. After treatments, the cells were analyzed for ERO1α protein expression (C); anti-β-actin antibody was used as a loading control, for Fluo 4- (D), Rhod 2- (E) and MitoSOX red- (F) fluorescence. The results represent the means ± SD calculated from at least three distinct experiments. (N.d., not detectable). *P < 0.05, **P < 0.01, as compared to untreated cells. (*) P < 0.05, (**) P < 0.01, as compared to cells treated with arsenite (ANOVA followed by Dunnett's test).

3.5. ISRIB inhibits ERO1α expression induced by arsenite.

Having established the cell type-independence of the above findings, as well as the notion that pharmacological inhibition of ERO1α provides effects in line with those observed in ERO KO cells, we performed other experiments using ISRIB, a small molecule that inhibits ERO1α expression (Sidrauski et al., 2015) (Rabouw et al., 2019a). In these experiments, RP-U937 and WT-C2C12 were exposed for 6 h to 2.5 µM arsenite, or 5 µM thapsigargin, either alone or combined with 0.2 µM ISRIB. As indicated in Fig. 10, arsenite and thapsigargin caused a similar increase in ERO1α expression in RP-U937 (Fig. 10A, C) and WT D-C2C12 (Fig. 10B, D), in both circumstances sensitive to ISRIB.

These results are in keeping with the well-established notion that validate that ISRIB is an effective inhibitor of ERO1α expression.

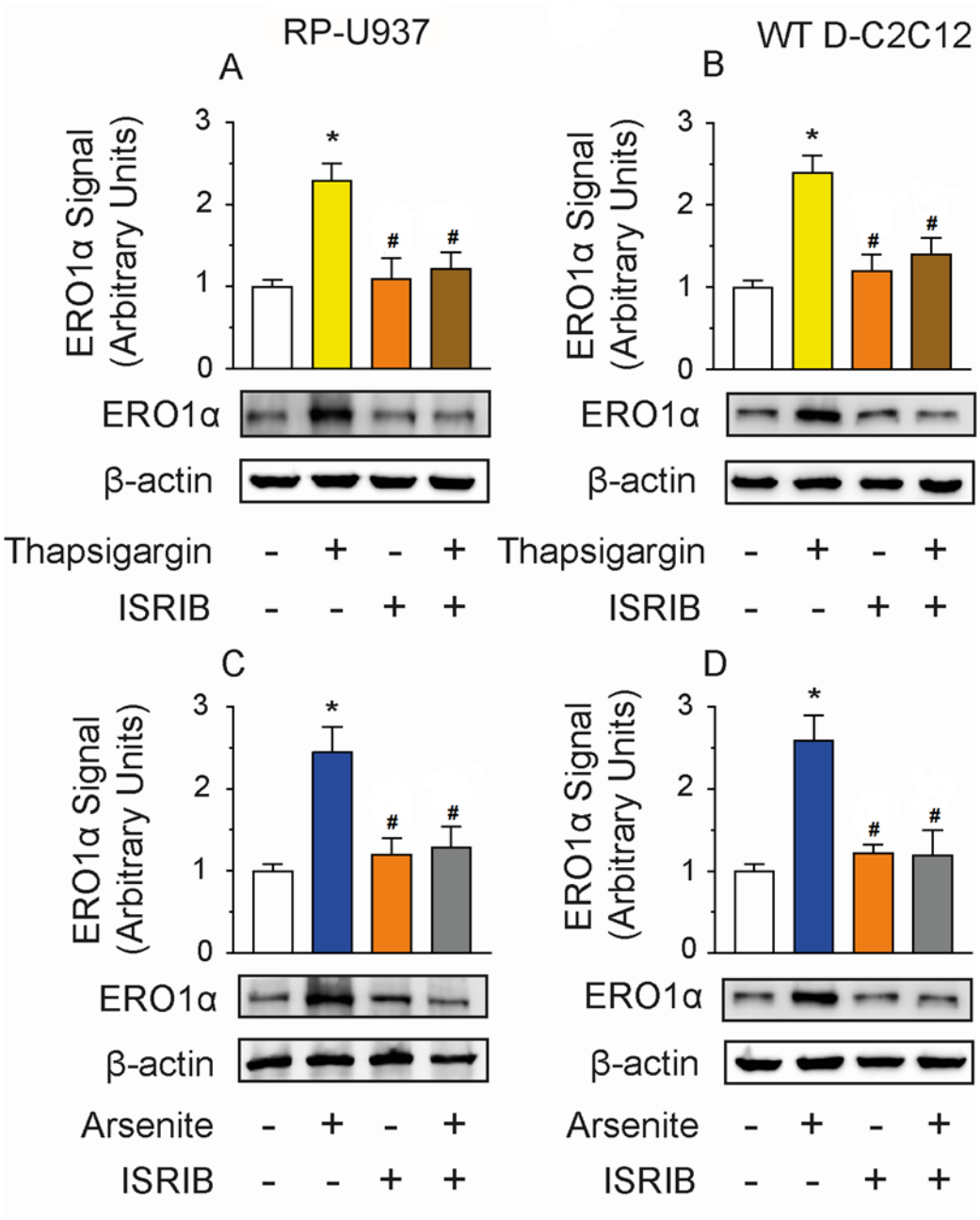

Figure 10. ISRIB inhibits ERO1α expression induced by thapsigargin or arsenite.

RP-U937 (A, C) and WT D-C2C12 (B, D) cells were exposed for 6 h to 5 μM thapsigargin (A, B) or arsenite (C, D), in the absence or presence of 0.2 μM ISRIB, and then analyzed for ERO1α protein expression. Anti-β-actin antibody was used as a loading control. Results represent the means ± SD calculated from three separate experiments. *P < 0.01, as compared to untreated cells. #P < 0.01, as compared to cells treated with thapsigargin or arsenite (ANOVA followed by Dunnett's test).

3.6. Pharmacological inhibition of ERO1α expression or activity, or its genetic deletion, abolishes the early deleterious effects of arsenite.

The effects of a 6 h exposure to 2.5 μM arsenite on the $[Ca^{2+}]_c$, $[Ca^{2+}]_m$ and mito$O_2^{\bullet-}$ formation in WT D-C2C12 and ERO1α KO D-C2C12, with or without 2-APB, Ry or EN460 supplementation, have been previously discussed and are also illustrated in Fig. 11A-C. Interestingly ISRIB, under the same conditions associated with inhibition of ERO1α expression, recapitulated all the effects mediated by EN460 or Ry (Fig. 11A-C). Based on these findings, we decided to test the role of ERO1α in arsenite toxicity using pharmacological inhibitors of ERO1α activity and expression or ERO1α KO cells.

RP-U937 and WT D-C2C12 were therefore incubated for increasing time intervals in the presence of EN460 or ISRIB and finally analyzed for cell viability. There was no evidence of toxicity in cells exposed to EN460 or ISRIB for 6 h, as determined by measuring the number of viable cells (Fig. 12A, B), loss of membrane integrity (Fig. 12C, D) and apoptotic DNA condensation/fragmentation (Fig. 12E, F). ISRIB did not exert detectable toxic effects even at the 16 h or 24 time-points. However, RP-U937 were remarkably susceptible to long term exposure to EN460, displaying a large increase in the number of both necrotic and apoptotic cells at 16 and 24 h. In contrast with these findings, arsenite failed to promote toxicity in WT D-C2C12 also at the 16 or 24 h time-points.

We therefore performed experiments measuring the effects of the above inhibitors on the genotoxicity induced by arsenite. We found that arsenite promotes the accumulation of similar levels of DNA single strand breaks in RP-U937 and WT D-C2C12 cells (Fig. 11D), in both circumstances prevented by Ry, ISRIB or EN460. ERO1α KO D-C2C12 cells were instead resistant to the genotoxic effects mediated by the metalloid. In other identical experiments, Cf (10 mM) was given to RP-U937, WT D-C2C12 and ERO1α KO D-C2C12 in the last 10 min of incubation. Under these conditions, there was a similar increase of the $[Ca^{2+}]_c$ (Fig. 11E), $[Ca^{2+}]_m$ (Fig. 11F), mito$O_2^{\bullet-}$ formation (Fig. 11G) and DNA strand scission (Fig. 11H) in the three different cell types. Also similar were the suppressive effects of Ry for three different parameters. Importantly, however, EN460 or ISRIB failed to recapitulate the inhibitory effects of Ry under these conditions.

The results presented in this section indicate that a 6 h exposure to EN460 and ISRIB fails to promote toxicity in RP-U937, WT D-C2C12 and ERO1α KO D-C2C12. Under these conditions, EN460 and ISRIB mimicked the protective effects of Ry on the DNA strand scission induced by arsenite. Consistently, ERO1α KO D-C2C12 were resistant to arsenite genotoxicity. We also demonstrated

that EN460 and ISRIB do not afford protective effects under conditions in which mitochondrial Ca^{2+} accumulation and mito$O_2^{\bullet-}$ formation is enforced *via* Cf supplementation. This observation implies that the inhibitory effects of EN460 and ISRIB are causally linked to inhibition of RyR activation after the initial IP_3R stimulation induced by arsenite.

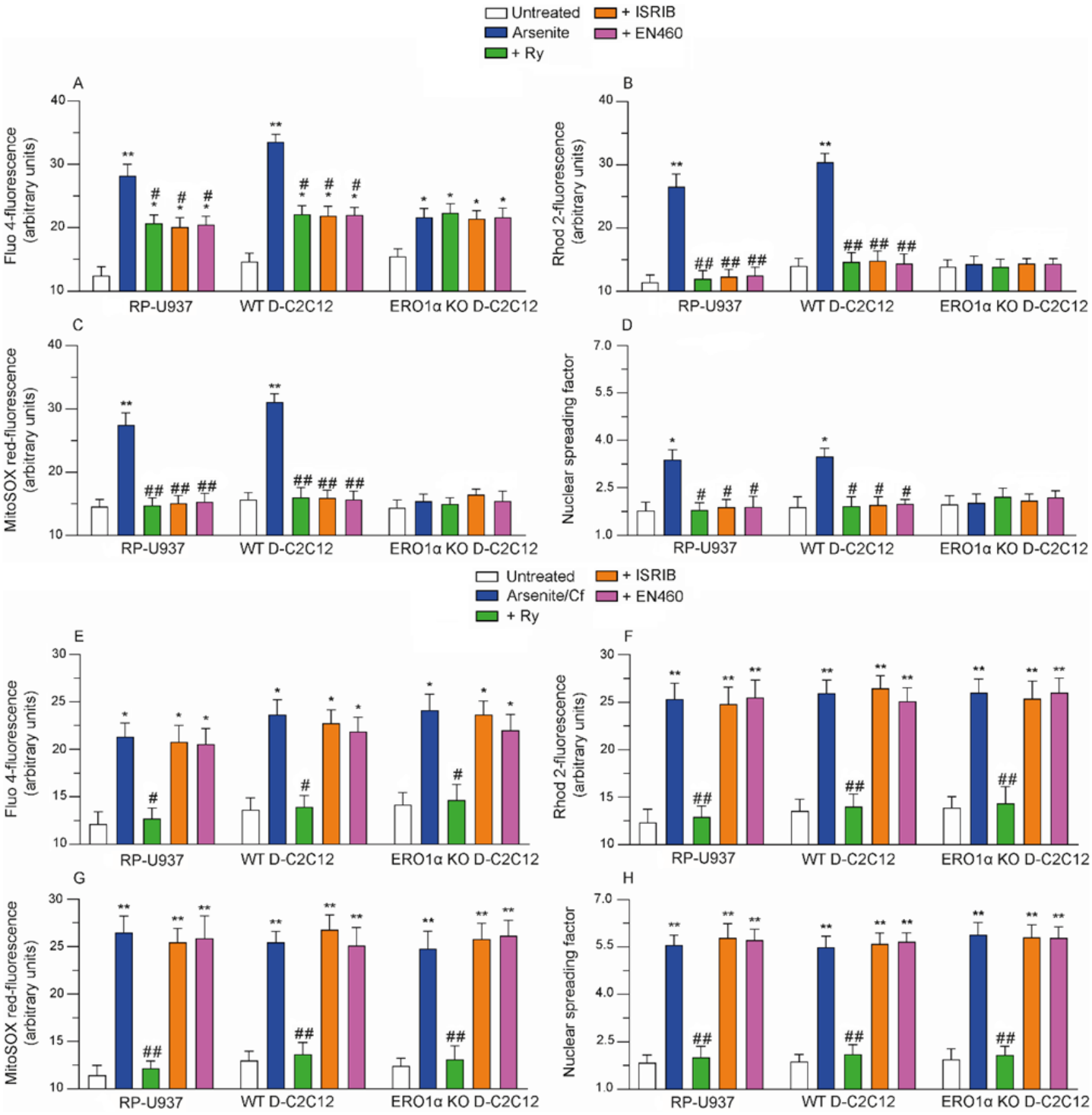

Figure 11. ISRIB and EN460 recapitulate the effects of ryanodine on the $[Ca^{2+}]_c$, $[Ca^{2+}]_m$, mitochondrial superoxide formation and DNA damage induced by arsenite.

U937, WT D-C2C12 and ERO1α KO D-C2C12 cells were pretreated for 5 min with the vehicle, Ry, ISRIB or EN460 and incubated for 6 h with the further addition to arsenite. After treatments, the cells were analyzed for Fluo 4- (A), Rhod 2- (B) and MitoSOX red- (C) fluorescence as well as for DNA damage with the alkaline halo assay (D). In other experiments, cells exposed for 6 h to ISRIB, or

EN460, were washed, re-suspended in fresh culture medium, loaded for 20 min with Fluo 4 (E), Rhod 2 (F), or MitoSOX red (G) and subsequently incubated for 10 min with 10 mM Cf and 2.5 µM arsenite. After treatments, the cells were analyzed for their respective fluorescence responses (E–G) and DNA damage (H). The results represent the means ± SD calculated from at least three distinct experiments. *P < 0.05, **P < 0.01, as compared to untreated cells. #P < 0.05, ## P < 0.01, as compared to cells treated with arsenite (ANOVA followed by Dunnett's test).

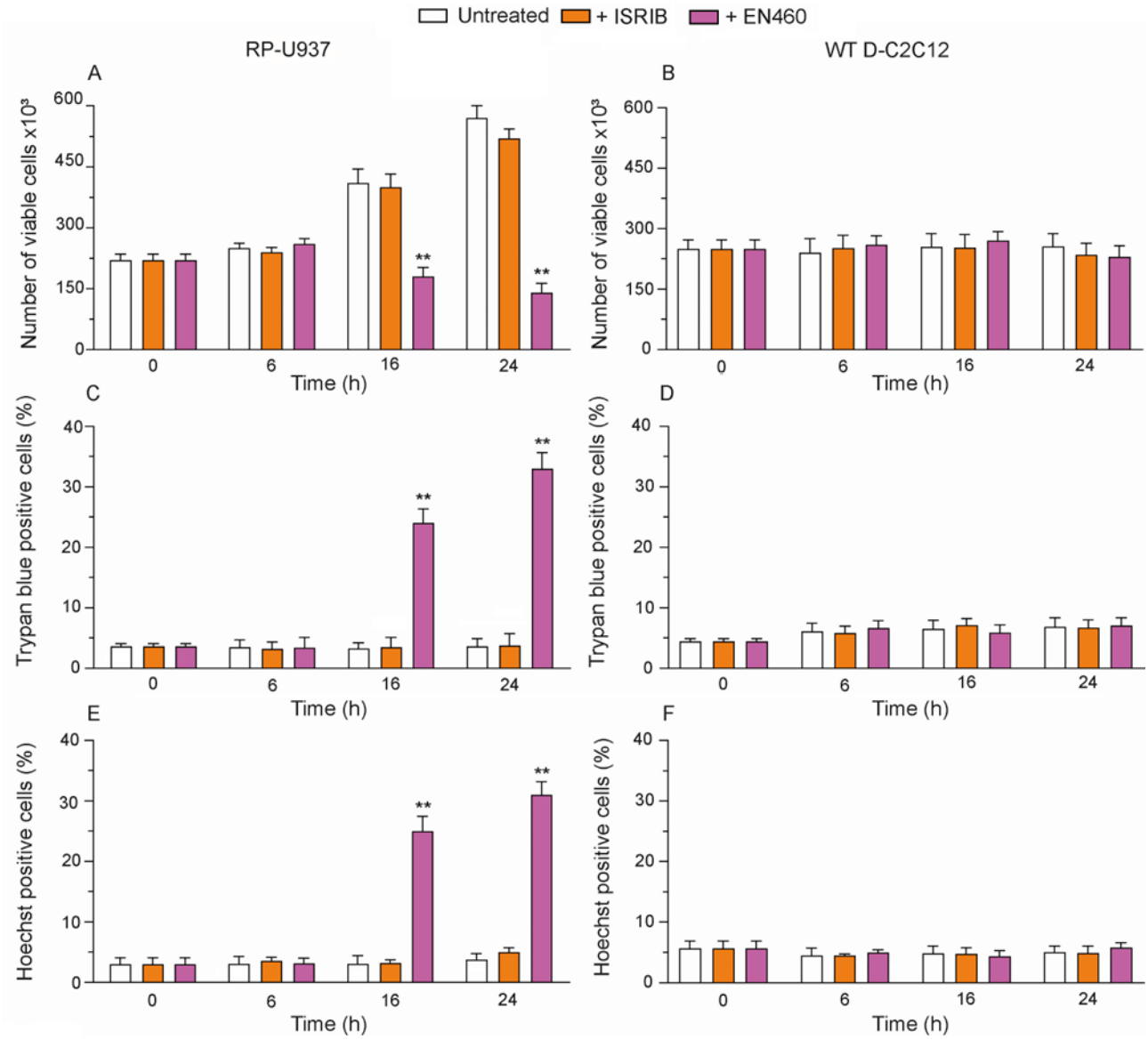

Fig. 12. The effects of ISRIB or EN460 on U937 and WT D-C2C12 cell viability.

U937 and WT D-C2C12 cells were exposed for increasing time intervals to ISRIB or EN460, and then analyzed by counting the number of viable cells (A) and trypan blue positive cells (B). Sister cultures were processed for the assessment of apoptotic chromatin fragmentation/condensation (C). The results represent the means ± SD calculated from at least three distinct experiments. *P < 0.05, **P < 0.01, as compared to untreated cells. (ANOVA followed by Dunnett's test).

3.7. Pharmacological inhibition of ERO1α expression or activity, or its genetic deletion, abolishes the delayed toxic effects of arsenite.

Prolonged exposure (16 h) of RP-U937 cells to 2.5 μM arsenite promotes a decline in mitochondrial membrane potential (Fig. 13A) and MTT reducing activity (Fig. 13B) as well as the mitochondrial loss of cytochrome c associated with a concomitant increase in the cytosol, detected in both Western blot (Fig. 13C) and immunofluorescence studies (Fig. 13D) (Fiorani et al., 2018) (Guidarelli et al., 2019). Similar effects were observed in WT D-C2C12 cells. ISRIB, or EN460, prevented all these toxic effects, thereby mimicking the effects of CsA, an immunosuppressor know to prevent MPT and MPT-dependent apoptosis (Bonora et al, 2014).

Next, we performed experiments in which RP-U937 and WT D-C2C12 were exposed to arsenite for 24 h, a condition associated with caspase 3 activations (Fig. 13E) and apoptotic chromatin fragmentation/condensation associated (Fig. 13F). These effects were invariably sensitive to CsA, ISRIB or EN460.

Arsenite failed to promote a reduction in mitochondrial membrane potential (Fig. 13A), MTT reducing activity (Fig. 13B), mitochondrial loss of cytochrome c (Fig. 13C, D) and to induce caspase 3 activation (Fig. 13E) and apoptotic DNA fragmentation (Fig. 13F) in ERO1α KO D-C2C12.

These results further emphasize the critical contribution of ERO1α in events associated with the regulation of Ca^{2+} homeostasis and mito$O_2^{\bullet-}$ formation and on downstream events triggered by mito$O_2^{\bullet-}$, as DNA strand scission and MPT-dependent cytotoxicity. It follows that chemical inhibition of ERO1α expression or activity represents an effective strategy to counteract the deleterious effects mediated by low concentrations of arsenite.

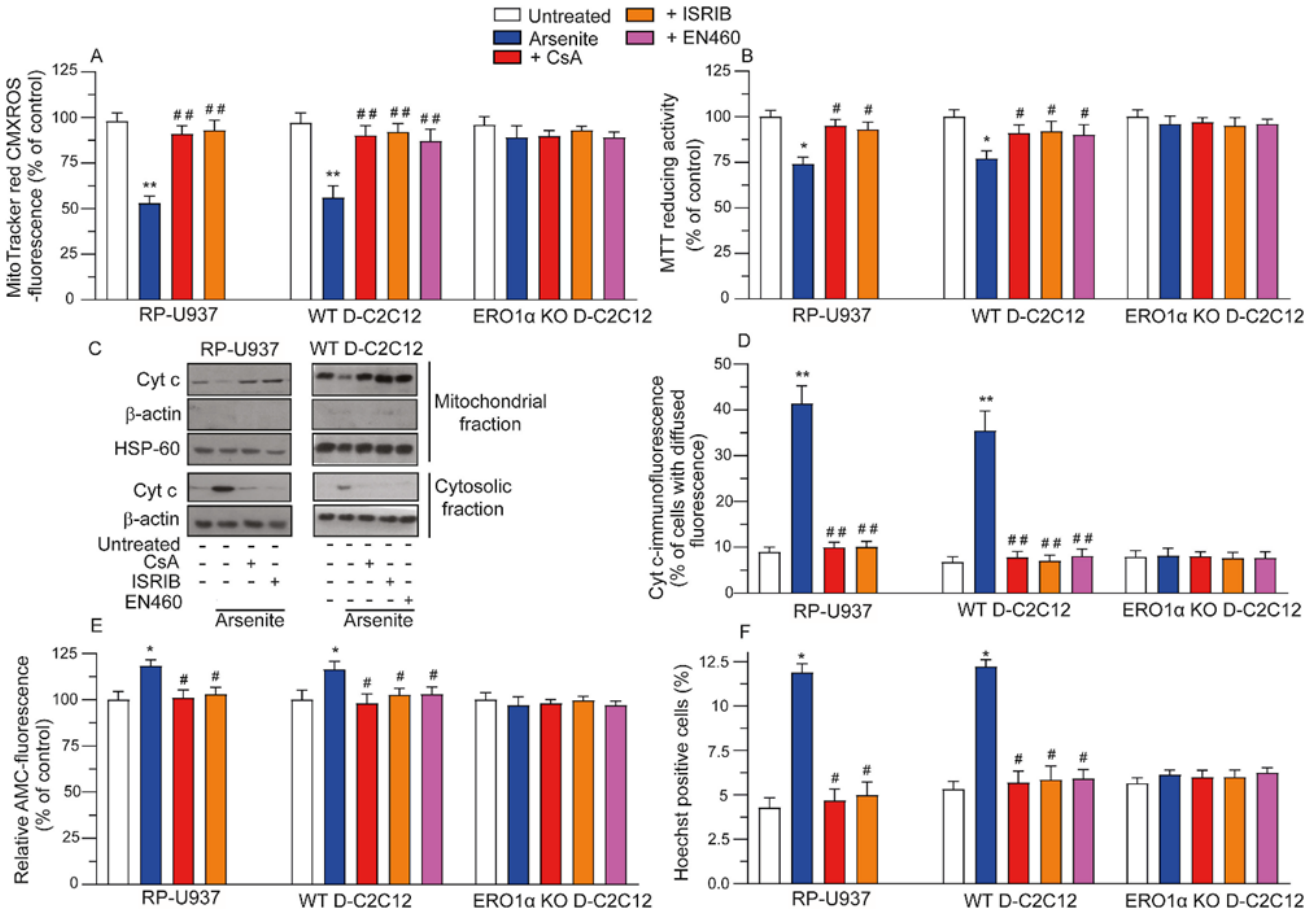

Figure 13. Arsenite causes mitochondrial dysfunction and apoptosis via mechanisms sensitive to inhibition of the activity or expression of ERO1α, as well as to its genetic deletion.

U937, WT D-C2C12 and ERO1α KO D-C2C12 cells were pretreated for 5 min with the vehicle, 0.5 μM CsA, ISRIB or EN460, and incubated for 16 (A–D) or 24 (E, F) h with arsenite. After treatments, the cells were analyzed for MitoTracker red CMXRos-fluorescence (A), MTT reducing activity (B), cytochrome c (Cyt c) immunoreactivity in the cytosolic and mitochondrial fractions (C), cytochrome c localization (D), caspase 3 activity (E), or apoptotic chromatin fragmentation/condensation (F). The results represent the means ± SD calculated from at least three distinct experiments. *P < 0.05, **P < 0.01, as compared to untreated cells. #P < 0.05, ##P < 0.01, as compared to cells treated with arsenite (ANOVA followed by Dunnett's test).

3.8. Mitochondrial superoxide contributes to ERO1α expression induced by arsenite.

As indicated above, arsenite induces ERO1α expression in RP-U937 cells *via* a mechanism blunted by 2-APB or ISRIB (Fig. 10C), and partially inhibited by Ry or EN460 (Fig. 8G). This indicates that IP_3R stimulation triggers the first mechanism of ERO1α expression (sensitive to 2-APB or ISRIB and insensitive to Ry or EN460). The partial inhibition of ERO1α expression mediated by Ry, or EN460, however implies the existence of a second mechanism regulated by RyR-derived Ca^{2+} and ERO1α activity. In order to obtain more information on this second mechanism, we performed additional experiments in RP-U937 cells and found that the inhibitory effects of Ry are mimicked by Ru360 (Fig. 14A), a MCU inhibitor (Bonora et al., 2014), thereby suggesting the involvement of mitochondrial Ca^{2+} accumulation and of the ensuing $mitoO_2^{\bullet-}$ formation. Indeed, Ru360 prevented both effects mediated by arsenite (Fig. 15B, C) with no apparent impact on the $[Ca^{2+}]_c$ (Fig. 15A). Interestingly, the second mechanism of ERO1α expression was also suppressed by rotenone (Fig. 15A), an inhibitor of mitochondrial complex I (Degli Esposti, 1998), which prevents $mitoO_2^{\bullet-}$ formation (Fig. 15C) in the absence of effects on the $[Ca^{2+}]_c$ (Fig. 15A) and $[Ca^{2+}]_m$ (Fig. 15B). Finally, the second mechanism of ERO1α expression was suppressed by AA (Fig. 14A), supplemented to the cells under conditions significantly increasing the content of the vitamin in the mitochondrial compartment. As previously demonstrated in our laboratory (Fiorani et al., 2015), RP-U937 cells express high-affinity transporters for AA in both the plasma and mitochondrial membranes, and their relative densities favors the accumulation of significant amounts of the vitamin in mitochondria. More specifically, short-term exposure to a low concentration of AA (e.g., 3 μM) increases the cytosolic and mitochondrial content of the vitamin reaching micromolar and millimolar levels, respectively. Thus, AA supplementation prevented $mitoO_2^{\bullet-}$ formation (Fig. 15C) in the absence of effects on the $[Ca^{2+}]_c$ (Fig. 15A) and $[Ca^{2+}]_m$ (Fig. 15B) and hampered the second mechanism of ERO1α expression.

The involvement of $mitoO_2^{\bullet-}$ in ERO1α expression was further established in experiments using RD-U937 cells, devoid of a functional mitochondrial respiratory chain and hence unable to release $mitoO_2^{\bullet-}$ in response to the metalloid (Fig. 15C). However, the effects of arsenite on Ca^{2+} homeostasis (Fig. 15D, E) were like those previously measured in their respiration proficient counterpart. RD-U937 cells responded to arsenite with a low increase in ERO1α, like that detected in RP-U937 cells supplemented with Ry. In addition, ERO1α expression was on the one hand suppressed by ISRIB and 2-APB and on the other hand insensitive to EN460, Ry, Ru360, rotenone and AA (Fig. 14B). Thus,

we were able to identify only one mechanism of ERO1α expression in RD-U937 cells exposed to arsenite, the one driven by IP_3R-dericed Ca^{2+}.

The results presented in this section provide evidence for the existence of two different mechanisms mediating ERO1α expression in U937 cells. The first one, critically implicated in RyR stimulation and mitochondrial Ca^{2+} accumulation, is caused by an ER stress response driven by IP_3R-derived Ca^{2+} whereas the second one appears to be entirely dependent on $mitoO_2^{\bullet-}$.

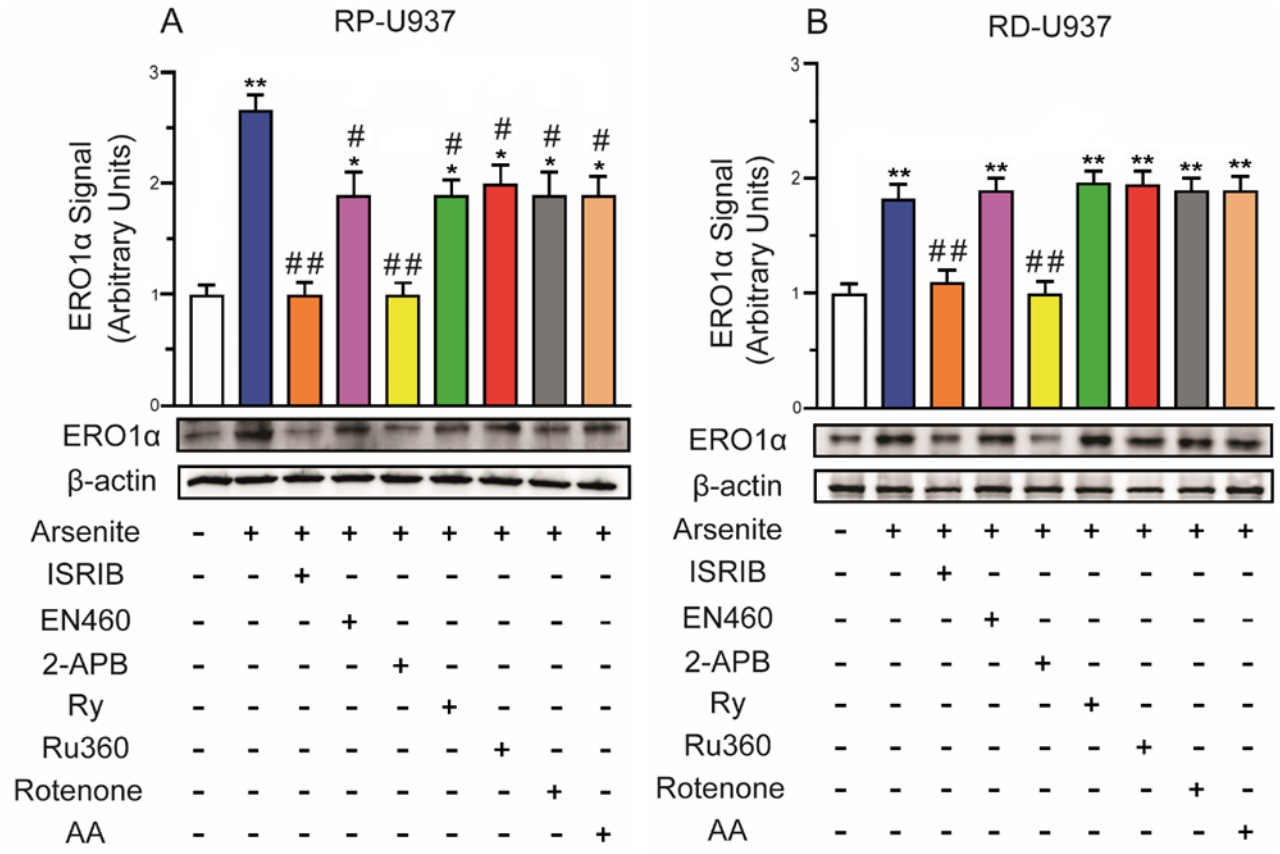

Figure 14. Pharmacological modulation of arsenite-induced ERO1α expression in respiration-proficient and respiration-deficient U937 cells.

RP-U937 (A) and RD-U937 (B) were pretreated for 5 min with the vehicle, with or without ISRIB, EN460, 2-APB, Ry, 10 μM Ru360 or 0.5 μM rotenone, and incubated for 6 h with the further addition to arsenite. In some experiments, the cells were treated for 15 min with 3 μM AA prior to arsenite supplementation. After treatments, the cells were analyzed for ERO1α protein expression, as detailed in the Methods section. Anti-β-actin antibody was used as a loading control. Results represent the means ± SD calculated from three separate experiments. *P < 0.05; **P < 0.01 compared with untreated cells. #P < 0.05; ## P < 0.01 compared with arsenite treated cells. (ANOVA followed by Dunnett's test).

3.9. ERO1α expression induced by arsenite *via* the ROS-dependent mechanism fails to affect Ca^{2+} homeostasis.

We asked the question of whether the mechanism of ERO1α expression mediated by mito$O_2^{\bullet-}$, as previously shown for the one driven by IP_3R-derived Ca^{2+}, has an impact on RyR activity or, more generally, on Ca^{2+} homeostasis. As previously shown, a 6 h exposure to 2.5 μM arsenite elevates the $[Ca^{2+}]_c$, *via* a mechanism suppressed by 2-APB or ISRIB and partially reduced by Ry and EN460 in RP-U937 (Fig. 15A). Interestingly, Ru360, rotenone or AA failed to affect the Ca^{2+} response mediated by the metalloid. Furthermore, Ru360 mimicked the effects of 2-APB and ISRIB on mitochondrial Ca^{2+} accumulation, with no apparent effects detected with rotenone or AA (Fig. 15B). Finally, arsenite caused a similar increase in the $Ca^{2+}]_c$ (Fig. 15D) and $[Ca^{2+}]_m$ (Fig. 15E) of RP- and RD-U937 cells with identical effects mediated by all the inhibitors.

Thus, various treatments and the respiration-deficient phenotype, previously shown to prevent mito$O_2^{\bullet-}$ formation, and the ensuing mechanism of ERO1α expression, failed to promote detectable effects on Ca^{2+} homeostasis.

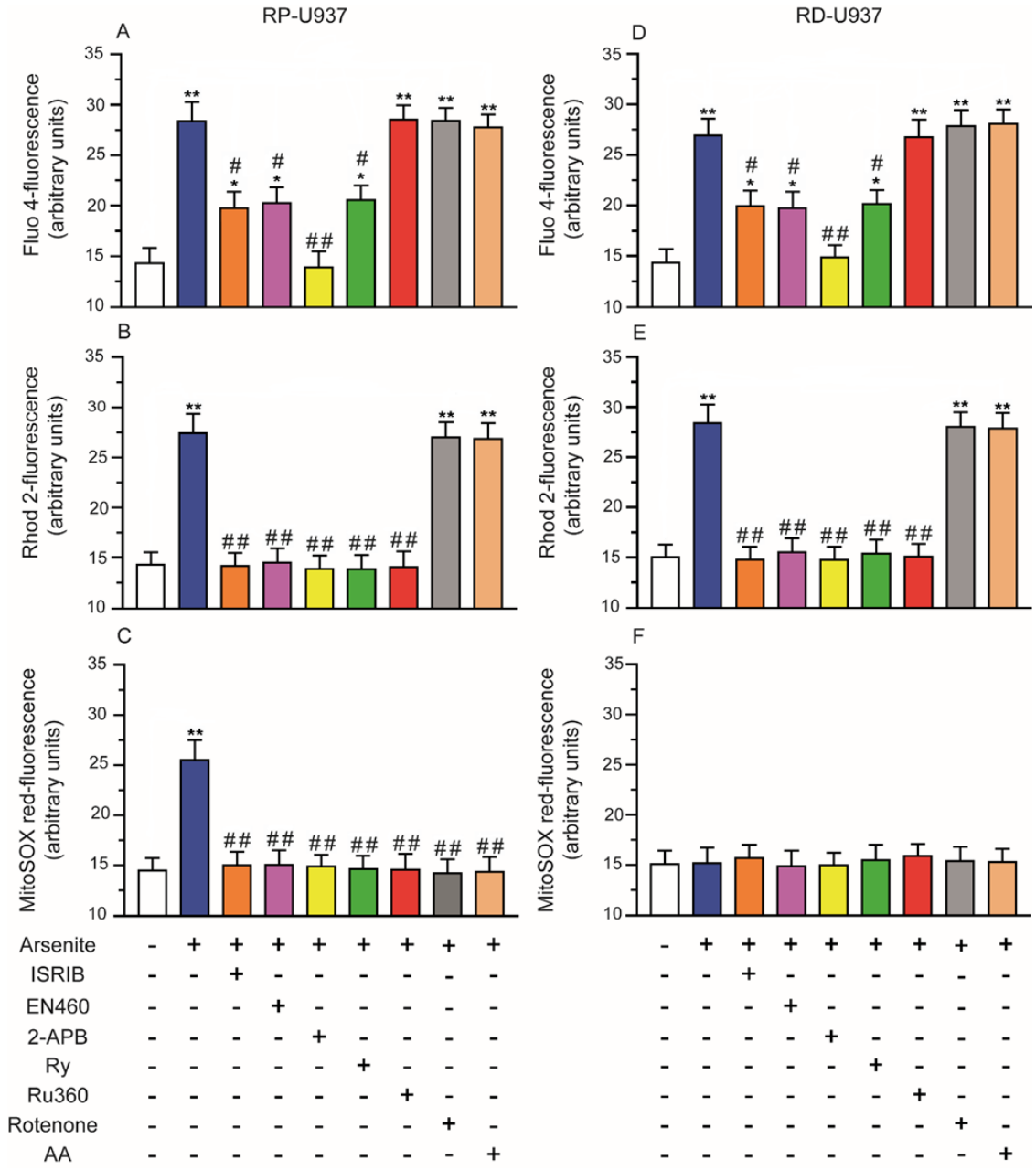

Figure 15. Pharmacological modulation of Ca^{2+} mobilization and mitochondrial accumulation, as well as mitochondrial superoxide formation, induced by arsenite in respiration-proficient and -deficient U937 cells.

RP-U937 (A-C) and RD-U937 (D-F) cells were pretreated for 5 min with the vehicle, ISRIB, EN460, 2-APB, Ry, Ru360 or rotenone, and incubated for 6 h with arsenite. In some experiments, the cells were treated for 15 min with AA prior to arsenite exposure. After treatments, the cells were analyzed for Fluo 4- (A, D), Rhod 2- (B, E) or MitoSOX red- (C, F) fluorescence. Results represent the means ± SD calculated from three separate experiments. *P < 0.05; **P < 0.01 compared with untreated cells. #P < 0.05; ## P < 0.01 compared with arsenite treated cells. (ANOVA followed by Dunnett's test).

3.10. The contribution of IP_3R-derived Ca^{2+} and mito$O_2^{\bullet-}$-derived H_2O_2 on the overall ER stress response.

The results presented in the previous section underscore the existence of two different mechanisms of ERO1α expression induced by arsenite, the first one driven by IP_3R-derived Ca^{2+} and the second by mito$O_2^{\bullet-}$ -derived H_2O_2. These results therefore suggest a role for both mechanisms in the arsenite-dependent ER stress response. This notion was experimentally established by showing that CHOP mRNA expression induced by arsenite in RP-U937 cells (2.5 μM, 6 h, Fig. 16), besides being suppressed by ISRIB and 2-APB, is partially and similarly reduced by Ry, Ru360, rotenone or AA. The partial inhibitory effect of Ry, Ru360, rotenone and AA, previously shown to prevent the formation of mito$O_2^{\bullet-}$, document an involvement of this species in the second mechanism regulating ERO1α expression.

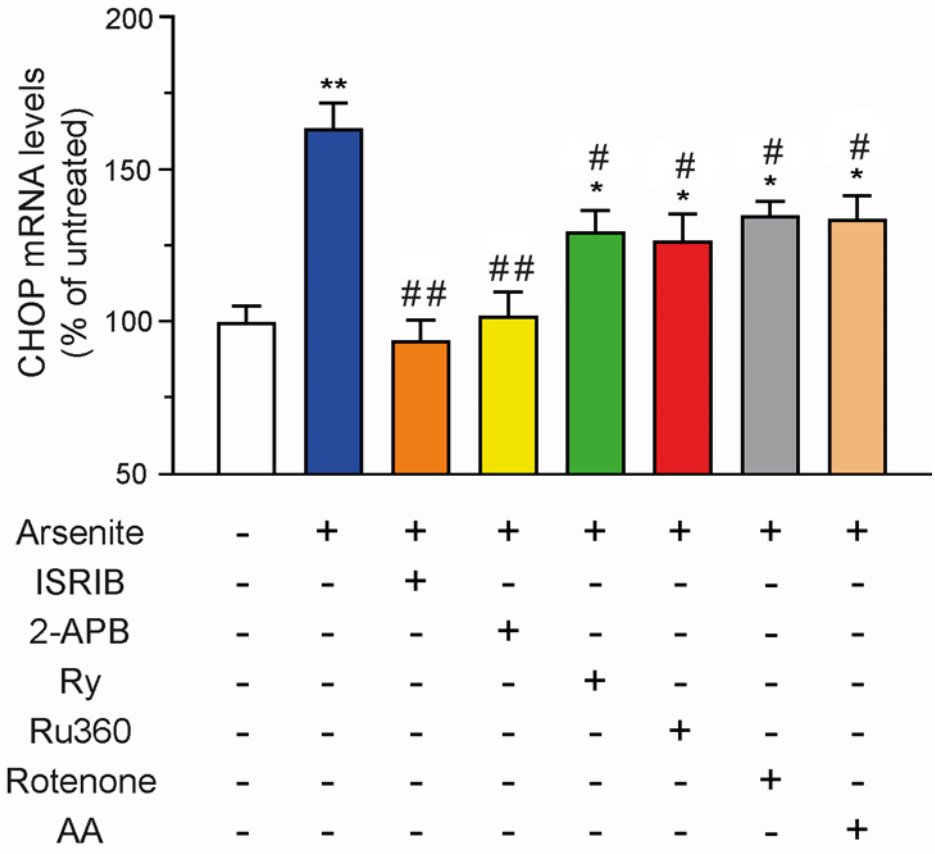

Figure 16. Pharmacological modulation of arsenite-induced CHOP mRNA expression in respiration-proficient U937 cells.

RP-U937 were pretreated for 5 min with the vehicle, ISRIB, 2-APB, Ry, Ru360 or rotenone, and incubated for 6 h with arsenite and analyzed for CHOP mRNA expression. Data are expressed with % respect to the untreated cells. Results represent the means ± SD calculated from three separate experiments. *P < 0.05; **P < 0.01 compared with untreated cells. #P < 0.05; ## P < 0.01 compared with arsenite treated cells. (ANOVA followed by Dunnett's test).

4. Discussion

Trivalent arsenic causes a plethora of deleterious effects in target cells, through its binding to protein thiols or *via* the intermediate formation of ROS mediated by various mechanisms. Recent work from our laboratory has focused on mito$O_2^{\bullet-}$ formation and demonstrated that this event is mediated by low concentrations of the metalloid in selected cell types *via* a Ca^{2+}-dependent mechanism (Guidarelli et al., 2021). We found that arsenite promotes mito$O_2^{\bullet-}$ formation in RP-U937 cells, or in other cell types expressing both the IP_3R and RyR, which were necessary to mediate mitochondrial Ca^{2+} accumulation (Guidarelli et al., 2021). There was no mitochondrial Ca^{2+} uptake in cells expressing only the IP_3R and therefore these cells failed to generate on mito$O_2^{\bullet-}$ in response to arsenite (Guidarelli et al., 2021).

Thus, arsenite caused an initial stimulation of the IP_3R sequentially connected with RyR activation and only the fraction of Ca^{2+} released by this second channel was taken up by the mitochondria to mediate ROS formation (Guidarelli et al., 2018) (Guidarelli et al., 2021).

An important issue addressed in this thesis work is related to the mechanism(s) linking IP_3R stimulation with RyR activation, apparently not mediated by a simple Ca^{2+}-induced Ca^{2+} release event, as the release of the cation from the first channel saturates at low arsenite concentrations, unlike Ca^{2+} release from the RyR, instead mediated by concentration-dependent mechanisms (Guidarelli et al., 2021).

We therefore tested the possibility of an involvement of ERO1α, a flavoprotein regulating under stress conditions various functions, including Ca^{2+} mobilization from the IP_3R and RyR (Anelli et al., 2013) (Hamilton et al., 2022). To address this issue, we initially employed a toxicity paradigm based on a 6 h exposure of RP-U937 cells to 2.5 μM arsenite and obtained evidence for an ER stress response characterized by increased expression of ATF4 and CHOP mRNA as well as of ERO1α protein.

We then performed inhibitor studies using EN460 and initially determined the conditions associated with inhibition of ERO1α activity in the absence of detectable toxic effects and/or other direct/indirect effects on Ca^{2+} homeostasis, in the absence of stimuli, or after agonist stimulation of Ca^{2+} release from the IP_3R and RyR.

Under these conditions, arsenite promoted an increase in the $[Ca^{2+}]_c$ and $[Ca^{2+}]_m$ *via* a mechanism respectively partially or completely inhibited by Ry. Mito$O_2^{\bullet-}$ formation taking place *via* the Ca^{2+}-

dependent mechanism was also suppressed by Ry as well as by EN460. Importantly, the effects mediated by Ry were validated by experiments performed in D-U937 cells, devoid of RyR.

These observations, suggesting the existence of a critical role of ERO1α in the regulation of RyR activation after the initial stimulation of the IP_3R, were next challenged in a different cell line with different characteristics, but nevertheless with a similar functional organization of the ER/mitochondria network (Guidarelli et al., 2021).

For this purpose, we used WT D-C2C12 cells, i.e., C2C12 cell-derived myotubes, providing Ca^{2+} and ROS responses to arsenite comparable to those observed in RP-U937 cells. The effects observed with EN460 under these conditions were also identical in the two cell types. Inhibition of ERO1α activity therefore recapitulated the effects associated with inhibition of Ca^{2+} release from the RyR. In addition, and, most importantly, we found that ERO1α KO D-C2C12 responded to arsenite as their WT counterpart supplemented with either Ry or EN460. Lack of ERO1α expression therefore confers resistance to the effects of arsenite associated with RyR activation, mitochondrial Ca^{2+} accumulation and mito$O_2^{\bullet-}$ formation.

The final approach to demonstrate the role of ERO1α in the Ca^{2+} responses induced by arsenite also involved the use of RP-U937 and WT D-C2C12 cells, however by replacing EN460 with ISRIB, an inhibitor of ERO1α expression. These experiments demonstrated that ISRIB blunts ERO1α expression as well as the increases in $[Ca^{2+}]_c$, $[Ca^{2+}]_m$ and mito$O_2^{\bullet-}$ induced by arsenite.

The first part of my work therefore provides a clear demonstration for the involvement of ERO1α in the RyR recruitment phase after the initial IP_3R stimulation induced by arsenite, an event critical for mitochondrial Ca^{2+} accumulation and the ensuing Ca^{2+}-dependent mito$O_2^{\bullet-}$ formation.

Interestingly, inhibition of the activity/expression as well as the genetic depletion of ERO1α also prevented the early genotoxic and late MPT-dependent apoptotic effects of arsenite.

The final question addressed in my work was on the mechanisms regulating ERO1α expression. Arsenite induces an ER stress response associated with an increased ERO1α expression driven by IP_3R-derived Ca^{2+} and by a second mechanism downstream to RyR activation, associated with mito$O_2^{\bullet-}$ formation. This second mechanism was therefore prevented by various treatments suppressing mito$O_2^{\bullet-}$ formation and was not observed in respiration-deficient cells. In addition, this second mechanism, failed to promote direct or indirect effects on Ca^{2+} homeostasis, an observation compatible with a different localization of the fractions of ERO1α generated by the two mechanisms. We therefore postulate that arsenite promotes “local” ER stress responses, driven by either IP_3R -

derived Ca^{2+} or $mitoO_2^{\bullet-}$ -derived H_2O_2, increasing the expression of ERO1α respectively in the MAMs, in the proximity of the RyR, or in microdomains distal from the MAMs and the Ry.

Collectively, our results (Fig. 17) demonstrate that a low concentration of arsenite uniquely generating $mitoO_2^{\bullet-}$ promotes direct effects on the IP_3R, causing Ca^{2+} release critically connected with an ER stress response associated with ERO1α expression. This fraction of ERO1α was then responsible for RyR activation and Ca^{2+} release in microdomains sensed by the mitochondria, thereby leading to $mitoO_2^{\bullet-}$ formation and to the ensuing geno- and cyto-toxicity. Pharmacological inhibition of the activity or expression of ERO1α, as its genetic deletion, was then invariably associated with prevention of all the deleterious effects mediated by the metalloid. We also underscored a second mechanism of ERO1α expression, driven by an ER stress caused by $mitoO_2^{\bullet-}$-derived H_2O_2, most likely in sites distal from the RyR and hence ineffectual for the regulation of Ca^{2+} homeostasis.

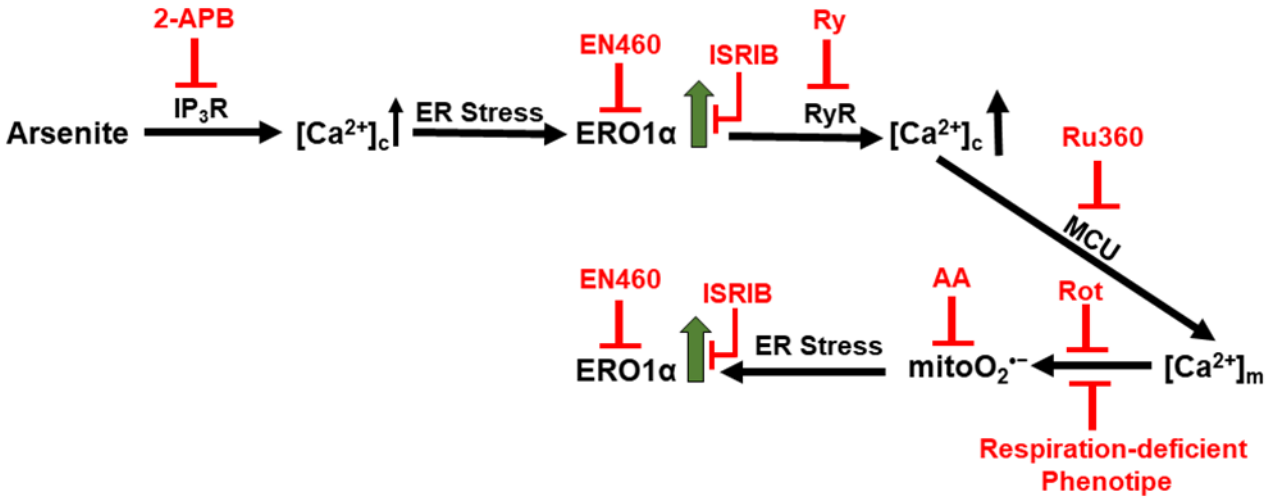

Figure 17: Mechanisms whereby arsenite increases ERO1α expression and ERO1α-dependent regulation of Ca^{2+} homeostasis and $mitoO_2^{\bullet-}$ formation.

5. Paper generated during PhD studies

Food and Chemical Toxicology 156 (2021) 112523

Contents lists available at ScienceDirect

Food and Chemical Toxicology

journal homepage: www.elsevier.com/locate/foodchemtox

Functional organization of the endoplasmic reticulum dictates the susceptibility of target cells to arsenite-induced mitochondrial superoxide formation, mitochondrial dysfunction and apoptosis

Andrea Guidarelli [a], Alessia Catalani [a], Andrea Spina [a], Ersilia Varone [b], Stefano Fumagalli [b], Ester Zito [b], Mara Fiorani [a], Orazio Cantoni [a,*]

[a] Department of Biomolecular Sciences, University of Urbino Carlo Bo, Urbino, Italy
[b] Istituto di Ricerche Farmacologiche Mario Negri IRCCS, Milan, Italy

Biochemical Pharmacology 198 (2022) 114973

Contents lists available at ScienceDirect

Biochemical Pharmacology

journal homepage: www.elsevier.com/locate/biochempharm

Crosstalk between ERO1α and ryanodine receptor in arsenite-dependent mitochondrial ROS formation

Andrea Spina [a,1], Andrea Guidarelli [a,1], Mara Fiorani [a], Ersilia Varone [b], Alessia Catalani [a], Ester Zito [a,b], Orazio Cantoni [a,*]

[a] Department of Biomolecular Sciences, University of Urbino Carlo Bo, Italy
[b] Istituto di Ricerche Farmacologiche Mario Negri IRCCS, Milan, Italy

Food and Chemical Toxicology 168 (2022) 113360

Contents lists available at ScienceDirect

Food and Chemical Toxicology

journal homepage: www.elsevier.com/locate/foodchemtox

Inhibition of activity/expression, or genetic deletion, of ERO1α blunts arsenite geno- and cyto-toxicity

Andrea Guidarelli [a], Andrea Spina [a], Mara Fiorani [a], Ester Zito [a,b], Orazio Cantoni [a,*]

[a] Department of Biomolecular Sciences, University of Urbino Carlo Bo, Urbino, Italy
[b] Istituto di Ricerche Farmacologiche Mario Negri IRCCS, Milan, Italy

Arsenite enhances ERO1α expression via ryanodine receptor dependent and independent mechanisms; Andrea Guidarelli, Andrea Spina, Mara Fiorani, Ester Zito, and Orazio Cantoni

Environmental Toxicology and Pharmacology – In revision

6. References

Almanza A, Carlesso A, Chintha C, Creedican S, Doultsinos D, Leuzzi B, Luís A, McCarthy N, Montibeller L, More S, Papaioannou A, Püschel F, Sassano ML, Skoko J, Agostinis P, de Belleroche J, Eriksson LA, Fulda S, Gorman AM, Healy S, Kozlov A, Muñoz-Pinedo C, Rehm M, Chevet E, Samali A. Endoplasmic reticulum stress signalling - from basic mechanisms to clinical applications. FEBS J. 2019 Jan;286(2):241-278. doi: 10.1111/febs.14608. Epub 2018 Aug 4. PMID: 30027602; PMCID: PMC7379631.

Anelli T, Bergamelli L, Margittai E, Rimessi A, Fagioli C, Malgaroli A, Pinton P, Ripamonti M, Rizzuto R, Sitia R. Ero1α regulates Ca(2+) fluxes at the endoplasmic reticulum-mitochondria interface (MAM). Antioxid Redox Signal. 2012 May 15;16(10):1077-87. doi: 10.1089/ars.2011.4004. Epub 2011 Oct 19. PMID: 21854214.

ATSDR, 2022. Substance Priority List (SPL). U.S. Department of Health and Human Services, Agency for Toxic Substances and Disease Registry, Atlanta, GA.

Bartok A, Weaver D, Golenár T, Nichtova Z, Katona M, Bánsághi S, Alzayady KJ, Thomas VK, Ando H, Mikoshiba K, Joseph SK, Yule DI, Csordás G, Hajnóczky G. IP3 receptor isoforms differently regulate ER-mitochondrial contacts and local calcium transfer. Nat Commun. 2019 Aug 19;10(1):3726. doi: 10.1038/s41467-019-11646-3. PMID: 31427578; PMCID: PMC6700175.

Basu A, Mahata J, Gupta S, Giri AK. Genetic toxicology of a paradoxical human carcinogen, arsenic: a review. Mutat Res. 2001 May;488(2):171-94. doi: 10.1016/s1383-5742(01)00056-4. PMID: 11344043.

Batke M, Afrapoli FM, Kellner R, Rathman JF, Yang C, Cronin MTD, Escher SE. Threshold of Toxicological Concern-An Update for Non-Genotoxic Carcinogens. Front Toxicol. 2021 Jun 24;3:688321. doi: 10.3389/ftox.2021.688321. PMID: 35295144; PMCID: PMC8915827.

Belzacq AS, El Hamel C, Vieira HL, Cohen I, Haouzi D, Métivier D, Marchetti P, Brenner C, Kroemer G. Adenine nucleotide translocator mediates the mitochondrial membrane permeabilization induced by lonidamine, arsenite and CD437. Oncogene. 2001 Nov 15;20(52):7579-87. doi: 10.1038/sj.onc.1204953. PMID: 11753636.

Berridge MJ. The Inositol Trisphosphate/Calcium Signaling Pathway in Health and Disease. Physiol Rev. 2016 Oct;96(4):1261-96. doi: 10.1152/physrev.00006.2016. PMID: 27512009.

Berridge MJ. Inositol trisphosphate and calcium signalling. Nature. 1993 Jan 28;361(6410):315-25. doi: 10.1038/361315a0. PMID: 8381210.

Blais JD, Chin KT, Zito E, Zhang Y, Heldman N, Harding HP, Fass D, Thorpe C, Ron D. A small molecule inhibitor of endoplasmic reticulum oxidation 1 (ERO1) with selectively reversible thiol reactivity. J Biol Chem. 2010 Jul 2;285(27):20993-1003. doi: 10.1074/jbc.M110.126599. Epub 2010 May 4. PMID: 20442408; PMCID: PMC2898301.

Bonora M, Pinton P. The mitochondrial permeability transition pore and cancer: molecular mechanisms involved in cell death. Front Oncol. 2014 Nov 17;4:302. doi: 10.3389/fonc.2014.00302. PMID: 25478322; PMCID: PMC4235083.

Bootman MD, Berridge MJ, Roderick HL. Calcium signalling: more messengers, more channels, more complexity. Curr Biol. 2002 Aug 20;12(16):R563-5. doi: 10.1016/s0960-9822(02)01055-2. PMID: 12194839.

Braakman I, Hebert DN. Protein folding in the endoplasmic reticulum. Cold Spring Harb Perspect Biol. 2013 May 1;5(5):a013201. doi: 10.1101/cshperspect.a013201. PMID: 23637286; PMCID: PMC3632058.

Cantoni O, Guidarelli A. Indirect mechanisms of DNA strand scission by peroxynitrite. Methods Enzymol. 2008;440:111-20. doi: 10.1016/S0076-6879(07)00806-3. PMID: 18423213.

Cantoni O, Zito E, Fiorani M, Guidarelli A. Arsenite impinges on endoplasmic reticulum-mitochondria crosstalk to elicit mitochondrial ROS formation and downstream toxicity. Semin Cancer Biol. 2021 Nov;76:132-138. doi: 10.1016/j.semcancer.2021.06.002. Epub 2021 Jun 3. PMID: 34089843.

Chen CJ, Chen CW, Wu MM, Kuo TL. Cancer potential in liver, lung, bladder and kidney due to ingested inorganic arsenic in drinking water. Br J Cancer. 1992 Nov;66(5):888-92. doi: 10.1038/bjc.1992.380. PMID: 1419632; PMCID: PMC1977977.

Chen, SJ., Yan, XJ., Chen, Z. (2013). Arsenic in Nature. In: Kretsinger, R.H., Uversky, V.N., Permyakov, E.A. (eds) Encyclopedia of Metalloproteins. Springer, New York, NY. https://doi.org/10.1007/978-1-4614-1533-6_489

Chin KT, Kang G, Qu J, Gardner LB, Coetzee WA, Zito E, Fishman GI, Ron D. The sarcoplasmic reticulum luminal thiol oxidase ERO1 regulates cardiomyocyte excitation-coupled calcium release and response to hemodynamic load. FASEB J. 2011 Aug;25(8):2583-91. doi: 10.1096/fj.11-184622. Epub 2011 Apr 20. PMID: 21507899; PMCID: PMC3136342.

Chong WC, Shastri MD, Eri R. Endoplasmic Reticulum Stress and Oxidative Stress: A Vicious Nexus Implicated in Bowel Disease Pathophysiology. Int J Mol Sci. 2017 Apr 5;18(4):771. doi: 10.3390/ijms18040771. PMID: 28379196; PMCID: PMC5412355.

Clemens MJ. Initiation factor eIF2 alpha phosphorylation in stress responses and apoptosis. Prog Mol Subcell Biol. 2001;27:57-89. doi: 10.1007/978-3-662-09889-9_3. PMID: 11575161.

National Research Council. 1999. Arsenic in Drinking Water. Washington, DC: The National Academies Press. https://doi.org/10.17226/6444.

Degli Esposti M. Inhibitors of NADH-ubiquinone reductase: an overview. Biochim Biophys Acta. 1998 May 6;1364(2):222-35. doi: 10.1016/s0005-2728(98)00029-2. PMID: 9593904.

De Stefani D, Patron M, Rizzuto R. Structure and function of the mitochondrial calcium uniporter complex. Biochim Biophys Acta. 2015 Sep;1853(9):2006-11. doi: 10.1016/j.bbamcr.2015.04.008. Epub 2015 Apr 18. PMID: 25896525; PMCID: PMC4522341.

Drahota P, Filippi M. Secondary arsenic minerals in the environment: a review. Environ Int. 2009 Nov;35(8):1243-55. doi: 10.1016/j.envint.2009.07.004. Epub 2009 Aug 7. PMID: 19665230.

Duchen MR. Mitochondria and calcium: from cell signalling to cell death. J Physiol. 2000 Nov 15;529 Pt 1(Pt 1):57-68. doi: 10.1111/j.1469-7793.2000.00057.x. PMID: 11080251; PMCID: PMC2270168.

Eisler R. Arsenic hazards to humans, plants, and animals from gold mining. Rev Environ Contam Toxicol. 2004;180:133-65. doi: 10.1007/0-387-21729-0_3. PMID: 14561078.

Eletto D, Chevet E, Argon Y, Appenzeller-Herzog C. Redox controls UPR to control redox. J Cell Sci. 2014 Sep 1;127(Pt 17):3649-58. doi: 10.1242/jcs.153643. Epub 2014 Aug 8. PMID: 25107370.

Eletto D, Eletto D, Dersh D, Gidalevitz T, Argon Y. Protein disulfide isomerase A6 controls the decay of IRE1α signaling via disulfide-dependent association. Mol Cell. 2014 Feb 20;53(4):562-576. doi: 10.1016/j.molcel.2014.01.004. Epub 2014 Feb 6. PMID: 24508390; PMCID: PMC3977204.

Fiorani M, Azzolini C, Cerioni L, Scotti M, Guidarelli A, Ciacci C, Cantoni O. The mitochondrial transporter of ascorbic acid functions with high affinity in the presence of low millimolar concentrations of sodium and in the absence of calcium and magnesium. Biochim Biophys Acta. 2015 Jun;1848(6):1393-401. doi: 10.1016/j.bbamem.2015.03.009. Epub 2015 Mar 15. PMID: 25786874.

Fiorani M, Guidarelli A, Cantoni O. Mitochondrial reactive oxygen species: the effects of mitochondrial ascorbic acid vs untargeted and mitochondria-targeted antioxidants. Int J Radiat Biol. 2021;97(8):1055-1062. doi: 10.1080/09553002.2020.1721604. Epub 2020 Feb 6. PMID: 31976796.

Fiorani M, Guidarelli A, Capellacci V, Cerioni L, Crinelli R, Cantoni O. The dual role of mitochondrial superoxide in arsenite toxicity: Signaling at the boundary between apoptotic commitment and cytoprotection. Toxicol Appl Pharmacol. 2018 Apr 15;345:26-35. doi: 10.1016/j.taap.2018.03.008. Epub 2018 Mar 8. PMID: 29526526.

Flora SJ. Arsenic-induced oxidative stress and its reversibility. Free Radic Biol Med. 2011 Jul 15;51(2):257-81. doi: 10.1016/j.freeradbiomed.2011.04.008. Epub 2011 Apr 13. PMID: 21554949.

Garrido C, Galluzzi L, Brunet M, Puig PE, Didelot C, Kroemer G. Mechanisms of cytochrome c release from mitochondria. Cell Death Differ. 2006 Sep;13(9):1423-33. doi: 10.1038/sj.cdd.4401950. Epub 2006 May 5. PMID: 16676004.

Giorgi C, Marchi S, Pinton P. The machineries, regulation and cellular functions of mitochondrial calcium. Nat Rev Mol Cell Biol. 2018 Nov;19(11):713-730. doi: 10.1038/s41580-018-0052-8. Erratum in: Nat Rev Mol Cell Biol. 2018 Sep 24;: PMID: 30143745.

Goyal MM, Basak A. Human catalase: looking for complete identity. Protein Cell. 2010 Oct;1(10):888-97. doi: 10.1007/s13238-010-0113-z. Epub 2010 Nov 9. PMID: 21204015; PMCID: PMC4875117.

Guha P, Kaptan E, Gade P, Kalvakolanu DV, Ahmed H. Tunicamycin induced endoplasmic reticulum stress promotes apoptosis of prostate cancer cells by activating mTORC1. Oncotarget. 2017 Jul 15;8(40):68191-68207. doi: 10.18632/oncotarget.19277. PMID: 28978108; PMCID: PMC5620248.

Guidarelli A, Catalani A, Spina A, Varone E, Fumagalli S, Zito E, Fiorani M, Cantoni O. Functional organization of the endoplasmic reticulum dictates the susceptibility of target cells to arsenite-induced mitochondrial superoxide formation, mitochondrial dysfunction and apoptosis. Food Chem Toxicol. 2021 Oct;156:112523. doi: 10.1016/j.fct.2021.112523. Epub 2021 Aug 25. PMID: 34453993.

Guidarelli A, Cerioni L, Fiorani M, Cantoni O. Differentiation-associated loss of ryanodine receptors: a strategy adopted by monocytes/macrophages to prevent the DNA single-strand breakage induced by peroxynitrite. J Immunol. 2009 Oct 1;183(7):4449-57. doi: 10.4049/jimmunol.0901260. Epub 2009 Sep 4. PMID: 19734222.

Guidarelli A, Fiorani M, Azzolini C, Cerioni L, Scotti M, Cantoni O. U937 cell apoptosis induced by arsenite is prevented by low concentrations of mitochondrial ascorbic acid with hardly any effect mediated by the cytosolic fraction of the vitamin. Biofactors. 2015 Mar-Apr;41(2):101-10. doi: 10.1002/biof.1204. Epub 2015 Mar 23. PMID: 25809564.

Guidarelli A, Fiorani M, Carloni S, Cerioni L, Balduini W, Cantoni O. The study of the mechanism of arsenite toxicity in respiration-deficient cells reveals that NADPH oxidase-derived superoxide promotes the same downstream events mediated by mitochondrial superoxide in respiration-proficient cells. Toxicol Appl Pharmacol. 2016 Sep 15;307:35-44. doi: 10.1016/j.taap.2016.07.012. Epub 2016 Jul 20. PMID: 27450018.

Guidarelli A, Fiorani M, Cerioni L, Cantoni O. Calcium signals between the ryanodine receptor- and mitochondria critically regulate the effects of arsenite on mitochondrial superoxide formation and on the ensuing survival vs apoptotic signaling. Redox Biol. 2019 Jan;20:285-295. doi: 10.1016/j.redox.2018.10.015. Epub 2018 Oct 23. PMID: 30388683; PMCID: PMC6216081.

Habib GM, Shi ZZ, Lieberman MW. Glutathione protects cells against arsenite-induced toxicity. Free Radic Biol Med. 2007 Jan 15;42(2):191-201. doi: 10.1016/j.freeradbiomed.2006.10.036. Epub 2006 Oct 12. PMID: 17189825; PMCID: PMC1855165.

Hamilton S, Terentyeva R, Bogdanov V, Kim TY, Perger F, Yan J, Ai X, Carnes CA, Belevych AE, George CH, Davis JP, Gyorke S, Choi BR, Terentyev D. Ero1α-Dependent ERp44 Dissociation From RyR2 Contributes to Cardiac Arrhythmia. Circ Res. 2022 Mar 4;130(5):711-724. doi: 10.1161/CIRCRESAHA.121.320531. Epub 2022 Jan 28. PMID: 35086342; PMCID: PMC8893133.

Hu Y, Li J, Lou B, Wu R, Wang G, Lu C, Wang H, Pi J, Xu Y. The Role of Reactive Oxygen Species in Arsenic Toxicity. Biomolecules. 2020 Feb 5;10(2):240. doi: 10.3390/biom10020240. PMID: 32033297; PMCID: PMC7072296.

Hughes MF. Arsenic toxicity and potential mechanisms of action. Toxicol Lett. 2002 Jul 7;133(1):1-16. doi: 10.1016/s0378-4274(02)00084-x. PMID: 12076506.

IARC, 2012. Monographs on the Evaluation of Carcinogenic Risks to Humans, Volume 100. ed. International Agency for Research on Cancer, Lyone, France.

Jomova K, Jenisova Z, Feszterova M, Baros S, Liska J, Hudecova D, Rhodes CJ, Valko M. Arsenic: toxicity, oxidative stress and human disease. J Appl Toxicol. 2011 Mar;31(2):95-107. doi: 10.1002/jat.1649. Epub 2011 Feb 14. PMID: 21321970.

Karagöz GE, Acosta-Alvear D, Walter P. The Unfolded Protein Response: Detecting and Responding to Fluctuations in the Protein-Folding Capacity of the Endoplasmic Reticulum. Cold Spring Harb Perspect Biol. 2019 Sep 3;11(9):a033886. doi: 10.1101/cshperspect.a033886. PMID: 30670466; PMCID: PMC6719602.

Kaur S, Kamli MR, Ali A. Role of arsenic and its resistance in nature. Can J Microbiol. 2011 Oct;57(10):769-74. doi: 10.1139/w11-062. Epub 2011 Sep 21. PMID: 21936668.

Kiviluoto S, Vervliet T, Ivanova H, Decuypere JP, De Smedt H, Missiaen L, Bultynck G, Parys JB. Regulation of inositol 1,4,5-trisphosphate receptors during endoplasmic reticulum stress. Biochim Biophys Acta. 2013 Jul;1833(7):1612-24. doi: 10.1016/j.bbamcr.2013.01.026. Epub 2013 Feb 1. PMID: 23380704.

Kosuri P, Alegre-Cebollada J, Feng J, Kaplan A, Inglés-Prieto A, Badilla CL, Stockwell BR, Sanchez-Ruiz JM, Holmgren A, Fernández JM. Protein folding drives disulfide formation. Cell. 2012 Nov 9;151(4):794-806. doi: 10.1016/j.cell.2012.09.036. PMID: 23141538; PMCID: PMC3506382.

Li G, Mongillo M, Chin KT, Harding H, Ron D, Marks AR, Tabas I. Role of ERO1-alpha-mediated stimulation of inositol 1,4,5-triphosphate receptor activity in endoplasmic reticulum stress-induced apoptosis. J Cell Biol. 2009 Sep 21;186(6):783-92. doi: 10.1083/jcb.200904060. Epub 2009 Sep 14. PMID: 19752026; PMCID: PMC2753154.

Lim KT, Shukor MY, Wasoh H. Physical, chemical, and biological methods for the removal of arsenic compounds. Biomed Res Int. 2014;2014:503784. doi: 10.1155/2014/503784. Epub 2014 Feb 17. PMID: 24696853; PMCID: PMC3947798.

Liochev SI, Fridovich I. The effects of superoxide dismutase on H2O2 formation. Free Radic Biol Med. 2007 May 15;42(10):1465-9. doi: 10.1016/j.freeradbiomed.2007.02.015. Epub 2007 Feb 28. PMID: 17448892.

Magnani ND, Marchini T, Calabró V, Alvarez S, Evelson P. Role of Mitochondria in the Redox Signaling Network and Its Outcomes in High Impact Inflammatory Syndromes. Front

Endocrinol (Lausanne). 2020 Sep 23;11:568305. doi: 10.3389/fendo.2020.568305. PMID: 33071976; PMCID: PMC7538663.

McQuiston A, Diehl JA. Recent insights into PERK-dependent signaling from the stressed endoplasmic reticulum. F1000Res. 2017 Oct 27;6:1897. doi: 10.12688/f1000research.12138.1. PMID: 29152224; PMCID: PMC5664976.

Meissner G. The structural basis of ryanodine receptor ion channel function. J Gen Physiol. 2017 Dec 4;149(12):1065-1089. doi: 10.1085/jgp.201711878. Epub 2017 Nov 9. PMID: 29122978; PMCID: PMC5715910.

Minatel BC, Sage AP, Anderson C, Hubaux R, Marshall EA, Lam WL, Martinez VD. Environmental arsenic exposure: From genetic susceptibility to pathogenesis. Environ Int. 2018 Mar;112:183-197. doi: 10.1016/j.envint.2017.12.017. Epub 2017 Dec 22. PMID: 29275244.

National Research Council (US) Subcommittee on Arsenic in Drinking Water. Arsenic in Drinking Water. Washington (DC): National Academies Press (US); 1999. 4, Health Effects of Arsenic

Onda Y. Oxidative protein-folding systems in plant cells. Int J Cell Biol. 2013;2013:585431. doi: 10.1155/2013/585431. Epub 2013 Sep 25. PMID: 24187554; PMCID: PMC3800646.

Oyadomari S, Mori M. Roles of CHOP/GADD153 in endoplasmic reticulum stress. Cell Death Differ. 2004 Apr;11(4):381-9. doi: 10.1038/sj.cdd.4401373. PMID: 14685163.

Pakos-Zebrucka K, Koryga I, Mnich K, Ljujic M, Samali A, Gorman AM. The integrated stress response. EMBO Rep. 2016 Oct;17(10):1374-1395. doi: 10.15252/embr.201642195. Epub 2016 Sep 14. PMID: 27629041; PMCID: PMC5048378.

Paul NP, Galván AE, Yoshinaga-Sakurai K, Rosen BP, Yoshinaga M. Arsenic in medicine: past, present and future. Biometals. 2022 Feb 21:1–19. doi: 10.1007/s10534-022-00371-y. Epub ahead of print. PMID: 35190937; PMCID: PMC8860286.

Rabouw HH, Langereis MA, Anand AA, Visser LJ, de Groot RJ, Walter P, van Kuppeveld FJM. Small molecule ISRIB suppresses the integrated stress response within a defined window of activation. Proc Natl Acad Sci U S A. 2019 Feb 5;116(6):2097-2102. doi: 10.1073/pnas.1815767116. Epub 2019 Jan 23. Erratum in: Proc Natl Acad Sci U S A. 2021 Apr 27;118(17): PMID: 30674674; PMCID: PMC6369741.

Ratnaike RN. Acute and chronic arsenic toxicity. Postgrad Med J. 2003 Jul;79(933):391-6. doi: 10.1136/pmj.79.933.391. PMID: 12897217; PMCID: PMC1742758.

Romero-Garcia S, Prado-Garcia H. Mitochondrial calcium: Transport and modulation of cellular processes in homeostasis and cancer (Review). Int J Oncol. 2019 Apr;54(4):1155-1167. doi: 10.3892/ijo.2019.4696. Epub 2019 Jan 28. PMID: 30720054.

Roy JS, Chatterjee D, Das N, Giri AK. Substantial Evidences Indicate That Inorganic Arsenic Is a Genotoxic Carcinogen: a Review. Toxicol Res. 2018 Oct;34(4):311-324. doi: 10.5487/TR.2018.34.4.311. Epub 2018 Oct 15. PMID: 30370006; PMCID: PMC6195883.

Rozpedek W, Pytel D, Mucha B, Leszczynska H, Diehl JA, Majsterek I. The Role of the PERK/eIF2α/ATF4/CHOP Signaling Pathway in Tumor Progression During Endoplasmic Reticulum Stress. Curr Mol Med. 2016;16(6):533-44. doi: 10.2174/1566524016666160523143937. PMID: 27211800; PMCID: PMC5008685.

Saha, J.C., Dikshit, A.K., Bandyopadhyay, M., Saha, K.C., 1999. A Review of Arsenic Poisoning and its Effects on Human Health. Crit. Rev. Environ. Sci. Technol. 29, 281–313. https://doi.org/10.1080/10643389991259227

Sapra A, Ramadan D, Thorpe C. Multivalency in the inhibition of oxidative protein folding by arsenic(III) species. Biochemistry. 2015 Jan 20;54(2):612-21. doi: 10.1021/bi501360e. Epub 2014 Dec 30. PMID: 25506675; PMCID: PMC4303313.

Sevier CS, Kaiser CA. Ero1 and redox homeostasis in the endoplasmic reticulum. Biochim Biophys Acta. 2008 Apr;1783(4):549-56. doi: 10.1016/j.bbamcr.2007.12.011. Epub 2007 Dec 23. PMID: 18191641.

Shaji, E., Santosh, M., Sarath, K. V, Prakash, P., Deepchand, V., Divya, B. V, 2021. Arsenic contamination of groundwater: A global synopsis with focus on the Indian Peninsula. Geosci. Front. 12, 101079. https://doi.org/https://doi.org/10.1016/j.gsf.2020.08.015

Shan J, Ord D, Ord T, Kilberg MS. Elevated ATF4 expression, in the absence of other signals, is sufficient for transcriptional induction via CCAAT enhancer-binding protein-activating transcription factor response elements. J Biol Chem. 2009 Aug 7;284(32):21241-8. doi: 10.1074/jbc.M109.011338. Epub 2009 Jun 9. PMID: 19509279; PMCID: PMC2755847.

Shen S, Li XF, Cullen WR, Weinfeld M, Le XC. Arsenic binding to proteins. Chem Rev. 2013 Oct 9;113(10):7769-92. doi: 10.1021/cr300015c. Epub 2013 Jun 28. PMID: 23808632; PMCID: PMC3797521.

Shergalis AG, Hu S, Bankhead A 3rd, Neamati N. Role of the ERO1-PDI interaction in oxidative protein folding and disease. Pharmacol Ther. 2020 Jun;210:107525. doi: 10.1016/j.pharmthera.2020.107525. Epub 2020 Mar 20. PMID: 32201313; PMCID: PMC7316501.

Sidrauski C, McGeachy AM, Ingolia NT, Walter P. The small molecule ISRIB reverses the effects of eIF2α phosphorylation on translation and stress granule assembly. Elife. 2015 Feb 26;4:e05033. doi: 10.7554/eLife.05033. PMID: 25719440; PMCID: PMC4341466.

Srivastava RK, Li C, Chaudhary SC, Ballestas ME, Elmets CA, Robbins DJ, Matalon S, Deshane JS, Afaq F, Bickers DR, Athar M. Unfolded protein response (UPR) signaling regulates arsenic trioxide-mediated macrophage innate immune function disruption. Toxicol Appl Pharmacol. 2013 Nov 1;272(3):879-87. doi: 10.1016/j.taap.2013.08.004. Epub 2013 Aug 14. PMID: 23954561; PMCID: PMC6028020.

Tournel G, Houssaye C, Humbert L, Dhorne C, Gnemmi V, Bécart-Robert A, Nisse P, Hédouin V, Gosset D, Lhermitte M. Acute arsenic poisoning: clinical, toxicological, histopathological, and

forensic features. J Forensic Sci. 2011 Jan;56 Suppl 1:S275-9. doi: 10.1111/j.1556-4029.2010.01581.x. Epub 2010 Oct 15. PMID: 20950314.

Valko M, Morris H, Cronin MT. Metals, toxicity and oxidative stress. Curr Med Chem. 2005;12(10):1161-208. doi: 10.2174/0929867053764635. PMID: 15892631.

Varone E, Pozzer D, Di Modica S, Chernorudskiy A, Nogara L, Baraldo M, Cinquanta M, Fumagalli S, Villar-Quiles RN, De Simoni MG, Blaauw B, Ferreiro A, Zito E. SELENON (SEPN1) protects skeletal muscle from saturated fatty acid-induced ER stress and insulin resistance. Redox Biol. 2019 Jun;24:101176. doi: 10.1016/j.redox.2019.101176. Epub 2019 Mar 23. PMID: 30921636; PMCID: PMC6438913.

Wang J, Pareja KA, Kaiser CA, Sevier CS. Redox signaling via the molecular chaperone BiP protects cells against endoplasmic reticulum-derived oxidative stress. Elife. 2014 Jul 22;3:e03496. doi: 10.7554/eLife.03496. PMID: 25053742; PMCID: PMC4132286.

Wang Y, Branicky R, Noë A, Hekimi S. Superoxide dismutases: Dual roles in controlling ROS damage and regulating ROS signaling. J Cell Biol. 2018 Jun 4;217(6):1915-1928. doi: 10.1083/jcb.201708007. Epub 2018 Apr 18. PMID: 29669742; PMCID: PMC5987716.

Waxman S, Anderson KC. History of the development of arsenic derivatives in cancer therapy. Oncologist. 2001;6 Suppl 2:3-10. doi: 10.1634/theoncologist.6-suppl_2-3. PMID: 11331434.

Winterbourn CC. Toxicity of iron and hydrogen peroxide: the Fenton reaction. Toxicol Lett. 1995 Dec;82-83:969-74. doi: 10.1016/0378-4274(95)03532-x. PMID: 8597169.

Yu W, Sanders BG, Kline K. RRR-alpha-tocopheryl succinate-induced apoptosis of human breast cancer cells involves Bax translocation to mitochondria. Cancer Res. 2003 May 15;63(10):2483-91. PMID: 12750270.

Zorov DB, Juhaszova M, Sollott SJ. Mitochondrial reactive oxygen species (ROS) and ROS-induced ROS release. Physiol Rev. 2014 Jul;94(3):909-50. doi: 10.1152/physrev.00026.2013. PMID: 24987008; PMCID: PMC4101632.